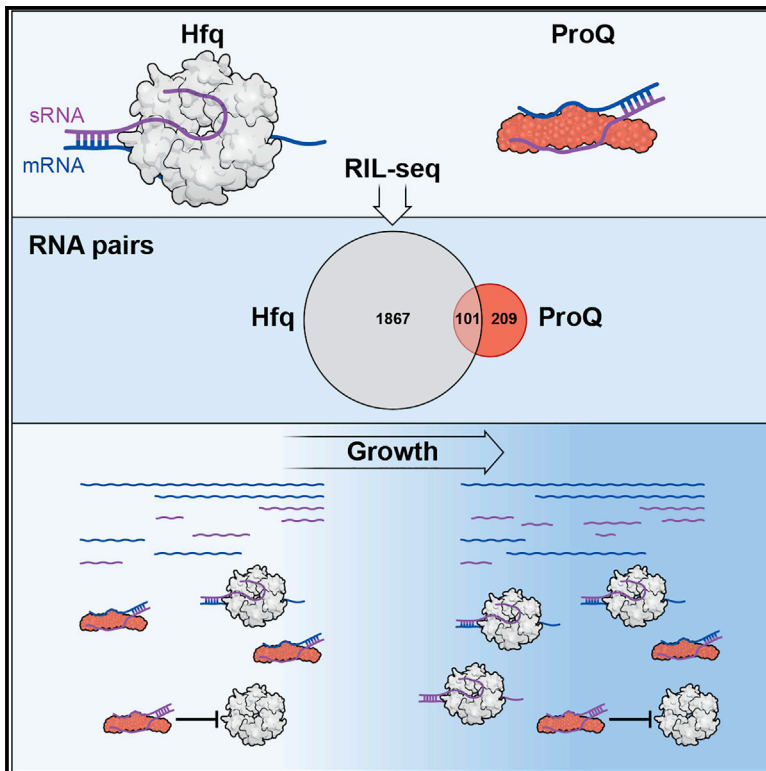


Molecular Cell

RNA-RNA Interactomes of ProQ and Hfq Reveal Overlapping and Competing Roles

Graphical Abstract



Authors

Sahar Melamed, Philip P. Adams,
Aixia Zhang, Hongen Zhang,
Gisela Storz

Correspondence

sahar.melamed@nih.gov (S.M.),
storzg@mail.nih.gov (G.S.)

In Brief

Melamed and Adams et al. compare the RNA-RNA interactomes of the well-characterized Hfq and the understudied ProQ RNA chaperones. They examine overlapping RNA pairs bound by both proteins, identify a new RNA sponge for the RybB small RNA, and document that ProQ can block Hfq activity.

Highlights

- RNA-RNA interactomes for RNA chaperones ProQ and Hfq are identified by RIL-seq
- A significant fraction of the RNA-RNA pairs on ProQ also are found on Hfq
- sRNA-mediated regulation is impacted by growth conditions
- ProQ blocks RNase III- and Hfq-mediated downregulation by a novel sRNA sponge



RNA-RNA Interactomes of ProQ and Hfq Reveal Overlapping and Competing Roles

Sahar Melamed,^{1,2,*} Philip P. Adams,^{1,2} Aixia Zhang,¹ Hongen Zhang,¹ and Gisela Storz^{1,3,*}

¹Division of Molecular and Cellular Biology, Eunice Kennedy Shriver National Institute of Child Health and Human Development, Bethesda, MD 20892-5430, USA

²These authors contributed equally

³Lead Contact

*Correspondence: sahar.melamed@nih.gov (S.M.), storzg@mail.nih.gov (G.S.)

<https://doi.org/10.1016/j.molcel.2019.10.022>

SUMMARY

Base pairing RNAs modulate gene expression in all studied organisms. In many bacteria, the base pairing between most small regulatory RNAs (sRNAs) and their targets is mediated by the Hfq RNA chaperone. However, recent studies have shown FinO-domain proteins also bind sRNAs. To examine the global contribution of the FinO-domain ProQ protein in *Escherichia coli*, we carried out RIL-seq to identify RNA pairs bound to this protein. The RNA-RNA interactome for ProQ contains hundreds of pairs. Intriguingly, a significant fraction of the ProQ-bound RNA pairs are also found associated with Hfq, indicating overlapping, complementary, or competing roles for the two proteins. Characterization of one novel RNA pair bound by both chaperones revealed that while Hfq is required for RNA sponge-mediated downregulation of the sRNA, ProQ can inhibit this regulation. Overall, our results uncover increased complexity in RNA regulatory networks involving RNA chaperone proteins, RNases, sRNAs, and mRNAs.

INTRODUCTION

It is now established that regulatory RNAs are integral to the cellular networks in most, if not all, organisms (reviewed in [Cech and Steitz, 2014](#)). In bacteria, the best-characterized group of regulatory RNAs are small RNAs (sRNAs) that act by limited base pairing with their target mRNAs, generally leading to changes in the translation and/or stability of the mRNAs (reviewed in [Wagner and Romby, 2015](#)).

In many bacteria, the RNA-binding chaperone Hfq is needed to promote efficient base pairing between the sRNA and its target (reviewed in [Updegrove et al., 2016](#); [Woodson et al., 2018](#)). An early key to understanding the global role of this regulator was the identification of sRNAs and mRNAs that co-immunoprecipitate with Hfq ([Sittka et al., 2008](#); [Zhang et al., 2003](#)). More recently, global insights into the sRNAs and their targets bound on Hfq have come from deep sequencing approaches (reviewed in [Hör et al., 2018](#); [Smirnov et al., 2017a](#)). One such

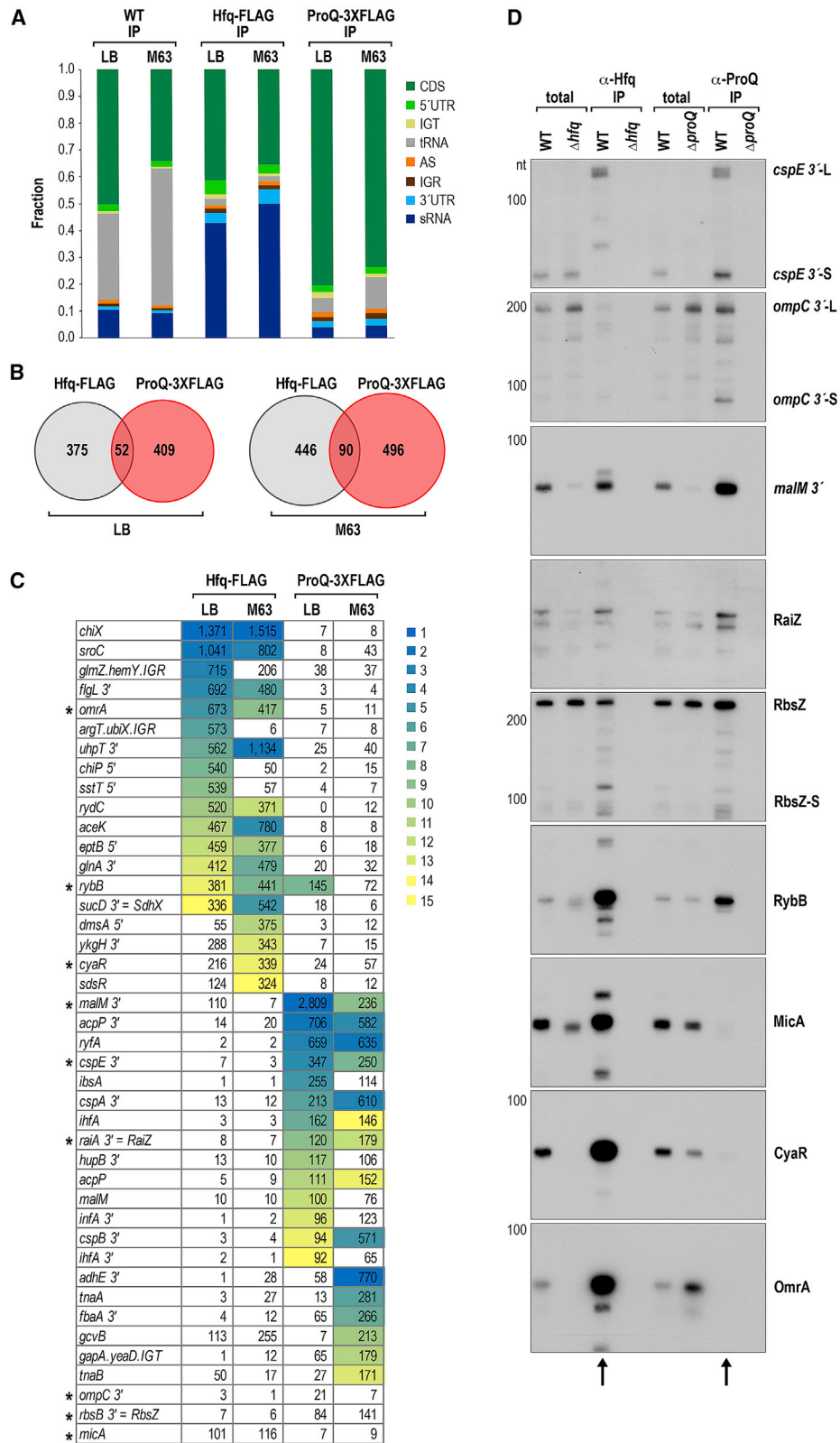
approach is RIL-seq (RNA interaction by ligation and sequencing) ([Melamed et al., 2016, 2018](#)). In RIL-seq, RNAs are crosslinked to the RNA-binding protein, and the protein is isolated by immunoprecipitation (IP). Proximal RNA ends are then ligated, giving rise to RNA chimeras, and the corresponding libraries are sequenced to identify both enriched and chimeric RNAs. This approach captured many of the previously known sRNA-target pairs and revealed new Hfq-mediated interactions in *Escherichia coli* ([Melamed et al., 2016](#)).

Recent studies have shown that proteins with a FinO domain constitute a second family of RNA chaperones in some bacteria (reviewed in [Olejniczak and Storz, 2017](#)). The *E. coli* F plasmid-encoded FinO was first shown to facilitate base pairing between the plasmid-encoded FinP sRNA and *traJ* mRNA ([Timmis et al., 1978](#); [van Biesen and Frost, 1994](#)), but similar RNA chaperone activities have now been reported for other family members ([Attaiech et al., 2016](#); [Chaulk et al., 2011](#)). The FinO-domain protein encoded on the *E. coli* chromosome is ProQ, so named because mutations in the corresponding gene led to increased resistance to the toxic protein analog 3,4-dehydro-D,L-proline ([Milner and Wood, 1989](#); [Stalmach et al., 1983](#)). The *proQ* gene product subsequently was found to decrease the osmoactivation of ProP, a transporter of compatible solutes including proline ([Kunte et al., 1999](#); [Milner and Wood, 1989](#)).

Co-IP experiments in *E. coli* and *Salmonella enterica* have shown ProQ binds many RNAs, including sRNAs ([Chaulk et al., 2011](#); [Holmqvist et al., 2018](#); [Smirnov et al., 2016, 2017b](#)). In *S. enterica*, the protein was reported to promote the base-pairing between the 3'-derived sRNAs RaiZ ([Smirnov et al., 2017b](#)) and STnc540 ([Westermann et al., 2019](#)) and their target mRNAs, leading to decreased levels of the encoded proteins. These data implicated ProQ as another RNA chaperone. Additionally, *S. enterica* ProQ was shown to protect the *cspE* mRNA from RNase II-mediated degradation ([Holmqvist et al., 2018](#)).

To further examine the cellular role of ProQ and to compare Hfq and ProQ, we applied RIL-seq to *E. coli* expressing FLAG-tagged derivatives of the RNA-binding proteins, generating comprehensive sets of the RNAs enriched and bound as pairs on each protein. We observed that while the ProQ interactome was smaller than that of Hfq, a third of the interactions were shared with Hfq. The formation of the shared chimeras was not dependent on one or the other chaperone as they were still observed in Δhfq and $\Delta proQ$ backgrounds. The most abundant ProQ-bound chimeras also found on Hfq included sRNAs and





(legend on next page)

mRNAs induced by osmotic and cell envelope stress conditions such as the σ^E -dependent sRNAs RybB and MicA. A detailed analysis of one of these regulatory interactions revealed that ProQ has additional roles such as blocking Hfq-mediated regulation.

RESULTS

RIL-Seq Analysis with Hfq-FLAG and ProQ-3XFLAG

To identify Hfq- and ProQ-associated RNAs and the corresponding RNA-RNA interactions, we carried out RIL-seq analysis with wild-type (WT) *E. coli* MG1655 cells expressing either Hfq-FLAG or ProQ-3XFLAG from the endogenous chromosomal locations. Cells were grown to $OD_{600} \sim 1.0$ in both rich (LB) and minimal (M63) glucose media and exposed to UV to crosslink the RNAs and proteins. After cell lysis, the Hfq-FLAG or ProQ-3XFLAG proteins were immunoprecipitated with their crosslinked RNAs (Figure S1A). RNA ends in close proximity were ligated, whereupon the RNA was isolated and used for the construction of cDNA libraries. As a control, cDNA libraries were similarly generated for WT cells not encoding tagged proteins but treated in an identical fashion. Each fragment in the cDNA library was sequenced from its two ends (pair-end sequencing) (Table S1). Analysis of the sequences resulted in two datasets: single fragments for which the two end sequences mapped to the same region of the genome and chimeric fragments for which the two end sequences mapped to two distinct regions of the genome due to the ligation of two RNAs in proximity to each other on Hfq or ProQ. We observed high correlations in the number of mapped sequence reads for same-condition libraries (Figure S1B).

Hfq and ProQ Generally Bind Different Sets of Individual RNAs

We first compared the RNAs bound by Hfq and ProQ (Table S2). For this analysis, all co-immunoprecipitated RNAs were analyzed, regardless of whether they were found in single or chimeric fragments. As expected, sRNAs and transcripts from 3' UTR regions that are likely to function as sRNAs were abundant in the Hfq datasets, as were mRNA coding sequences (CDS), which usually serve as targets (Figure 1A). In contrast, in the ProQ datasets, the sRNA fraction was low, and the largest fraction was comprised of CDS.

Analysis of the RNAs, which were most enriched relative to total RNA levels (≥ 15 -fold) for each set, revealed that while there was an overlap between the Hfq- and ProQ-bound RNAs, a unique set was enriched for each of the proteins, in both LB and M63 (Figure 1B). In the Hfq dataset, the 15 top-enriched RNAs were known sRNAs, sRNA candidates, and a few known sRNA targets (Figure 1C). For ProQ, many of the top enriched RNAs came from the 3' UTR regions of genes and toxin mRNAs (Figure 1C). Among these were the 3' UTRs of *raiA* and *infA*, which correspond to RaiZ and STnc540, the two *S. enterica* ProQ-dependent sRNAs characterized thus far (Smirnov et al., 2017b; Westermann et al., 2019). One sRNA, RybB, was found among the top 15 enriched RNAs in both datasets. While additional known and putative sRNAs were also enriched for both proteins (*malM* 3' and *CyaR*), others were only enriched for Hfq (*ChiX* and *RydC*) or ProQ (*RyfA* and *ibsA*). Among three additional RNAs characterized in more detail below, *ompC* 3' was only enriched for ProQ, *rbsB* 3' (renamed *RbsZ*) was significantly enriched with ProQ but also showed some enrichment with Hfq, and *MicA* was most enriched on Hfq.

In general, the absence of most of the Hfq-dependent sRNAs from the top of the list of ProQ is consistent with the previous reports that RNAs bound by ProQ differ from those bound by Hfq (Holmqvist et al., 2018; Smirnov et al., 2016). A comparison of the top ProQ-enriched RNAs in LB in our study to the 388 *E. coli* RNAs found crosslinked to ProQ using CLIP-seq (Holmqvist et al., 2018) showed that there was a 64% overlap for RNAs with a RIL-seq enrichment of ≥ 60 -fold (Table S3). The differences that are observed between the two datasets, such as less of an enrichment for 3' UTR sequences in the RIL-seq data, could be due to differences in strains and growth conditions as well as in the experimental and computational analyses.

To confirm the sRNA-binding observed in the RIL-seq data with tagged proteins, we isolated total RNA as well as RNA that co-immunoprecipitated with antibodies against the native forms of Hfq or ProQ from WT, Δhfq , and $\Delta proQ$ strains and examined the levels of known and candidate sRNAs in these samples (Figure 1D). For the sRNAs examined, the northern analysis supported the RIL-seq data, with some sRNAs enriched only with ProQ (*cspE* 3'-S and *ompC* 3'-S) or Hfq (*MicA*, *OmrA* and *CyaR*) and others enriched upon IP with both, though some stronger with ProQ (*malM* 3') or Hfq (*RybB*). The effects of deleting either *hfq* or *proQ* on the sRNA levels also varied. The levels

Figure 1. Unique Sets of RNAs Are Enriched on Hfq and ProQ

- (A) Distribution of RNAs derived from various genomic elements showing that the Hfq dataset is enriched for coding sequences (CDS) and sRNAs, while the ProQ dataset is enriched for CDS. Single and chimeric fragments from FLAG negative control, Hfq-FLAG, and ProQ-3XFLAG samples for cells grown in LB and M63 are classified into eight categories: CDS (coding sequence), 5' UTR, IGT (regions of an operonic transcript between genes), tRNA, AS (antisense transcript), IGR (intergenic region), 3' UTR, and sRNA. rRNA-derived fragments were excluded. Precise definitions of categories are in STAR Methods.
- (B) Venn diagram showing 11%–17% of the RNAs (IP enrichment ≥ 15) on Hfq-FLAG and ProQ-3XFLAG are shared in the different datasets.
- (C) The top 15 most-enriched RNAs on Hfq-FLAG and ProQ-3XFLAG are mostly similar between growth conditions but differ between the two chaperones. The IP enrichment value is given with the boxes for the top 15 most-enriched RNAs shaded according to the key. RNAs examined by northern analysis in Figures 1D and 2A are indicated by the asterisks.
- (D) Northern analysis of selected RNAs supports RIL-seq data for single RNAs. WT (GSO982), Δhfq (GSO954), and $\Delta proQ$ (GSO956) cells were grown to $OD_{600} \sim 1.0$ after a 1:100 dilution of the overnight culture and lysed, and Hfq or ProQ was immunoprecipitated by α -Hfq or α -ProQ antiserum, respectively. RNA was extracted from corresponding total lysates as well as immunoprecipitated samples, separated on an acrylamide gel, transferred to a membrane, and probed for the indicated RNAs (RNAs were probed sequentially on the same membrane). Size markers are indicated for all RNAs except where the portion of the blot shown is less than 100 nt. Prominent fragments for *cspE* and *ompC* 3' UTRs are denoted long (-L) and short (-S). Arrows point to co-IP lanes. The numbers in (C) represent the composite of multiple bands, while (D) documents differential Hfq and ProQ binding to the individual transcripts.

of a few sRNAs were not dramatically altered in either deletion strain (RbsZ), whereas others were more reduced in strains lacking either Hfq (OmrA, CyaR) or ProQ (*cspE* 3'-S) or both (*malM* 3'). We observed processed products, some of which also co-immunoprecipitated with the chaperones, for most of these sRNAs. Overall, this analysis showed that RIL-seq data can be used for characterizing the enrichment for RNAs in addition to the identification of RNA pairs.

***Δhfq* and *ΔproQ* Differentially Impact sRNA and mRNA Levels across Growth**

Given the varied effects of the *hfq* or *proQ* deletions on sRNA levels at one time point in growth, we carried out northern analysis to examine the consequences of deleting *hfq*, *proQ*, or both across growth. Since the *Δhfq* and double mutant strains have different growth curves reaching a lower final OD₆₀₀ (Figure S2A), samples were collected at specific times after dilution (60, 150, 210, and 360 min) corresponding to early, middle, and late exponential and stationary phases (Figure 2A). Each sRNA exhibited a distinct pattern in the different strains. The *cspE* 3'-S and *ompC* 3' levels were reduced at all points in growth in the *ΔproQ* strains, and the CyaR and OmrA levels were dramatically lower in the *Δhfq* mutant strains as expected (Schu et al., 2015). In contrast, the effects of *Δhfq* and *ΔproQ* were additive for *malM* 3' and RaiZ as well as for the known Hfq-binding RNAs RybB and MicA. We did note a slower migrating form of RybB that was more prevalent in the *Δhfq* backgrounds. Additionally, at 150 min of growth, MicA levels were elevated in *Δhfq* compared to the WT sample, possibly due to transcription induction by σ^E in the *Δhfq* background (Thompson et al., 2007). Overall, this analysis reinforces the conclusion that individual sRNAs are differentially affected by the lack of Hfq and ProQ and that this can vary across growth.

To examine the consequences of deleting *proQ* on a genome-wide level, we compared the transcriptomes of WT and *ΔproQ* strains at OD₆₀₀ ~1.0 (Figures 2B and S2B; Table S4). Only a small fraction of RNAs showed a change of ≥ 2 -fold in *ΔproQ* libraries compared to the WT libraries. However, it is noteworthy that among the RNAs whose expression changed ≥ 2 -fold, several were regulated by the EnvZ-OmpR two-component system, which activates and represses genes in response to fluctuations in osmotic pressure. Among the EnvZ-OmpR-regulated transcripts whose levels were elevated in *ΔproQ* compared to WT are the sRNA OmrA and the mRNA encoding the outer membrane protein OmpC. In contrast, the levels of the EnvZ-OmpR-

repressed mRNA encoding the outer membrane protein OmpF were decreased. These changes were also observed at specific points across growth by northern analysis (Figures 2A and 2C). Some *ΔproQ*-dependent induction of the *ompC* mRNA was still observed in a *ΔompR* background. Thus, while *ΔproQ* activates the OmpR-mediated stress response, part of the ProQ effects are independent of OmpR (Figure S2C). We also noted that while the levels of the *ompC* full-length mRNA increase (Figure 2C), the levels of fragments from the *ompC* 3' UTR decrease in the *ΔproQ* mutant (Figure 2A). Together these data show that ProQ impacts the expression of osmotic stress-inducible genes consistent with the reported *ΔproQ* sensitivity to osmotic stress (Kerr et al., 2014) and again support the conclusion that ProQ differentially affects individual transcripts from the same genetic region.

Abundance of 3' UTR Fragments Depends on ProQ but Not RNase II

The discordant effect of *ΔproQ* on the 3' UTR fragments and *ompC* mRNA (Figures 2A and 2C, respectively), combined with the fact that over half of the top 15 transcripts enriched on ProQ datasets correspond to 3' UTRs, led us to also examine the levels of the full-length and 3' UTR fragments for the *hupB* RNA. This 3' UTR was one of the most enriched transcripts on ProQ (Figure 1C). As for *ompC*, the levels of the full-length *hupB* transcripts were higher in the *ΔproQ* backgrounds at later points in growth, while the 3' UTR fragment was absent at all time points in the absence of ProQ (Figure 2D).

Given that ProQ was previously found to protect the *cspE* mRNA against RNase II-mediated cleavage (Holmqvist et al., 2018), we examined the effect of deleting the RNase II-encoding *mb* gene in both WT and *ΔproQ* backgrounds on both the full-length RNAs and 3' UTR fragments (Figures 2E and S2D). Similar to what has been reported for *S. enterica* (Holmqvist et al., 2018), *Δmb* partially suppressed the negative effect of the *ΔproQ* mutant for full-length *cspE*. Interestingly, the ratio of the two bands detected for full-length *hupB* was altered in *ΔproQ* compared to WT. Although the reason for this difference is not known, the levels were not strongly affected by the lack of RNase II. While full-length *ompC* levels were somewhat decreased in the *Δmb* background, the *Δmb* mutation did not eliminate the *ΔproQ*-dependent increase in *ompC* mRNA. For the three corresponding *cspE*, *hupB*, and *ompC* 3' UTR fragments, *Δmb* also did not suppress the effects of *ΔproQ*. Combined with the IP enrichment data, these results suggest that ProQ is binding to

Figure 2. sRNA and mRNA Levels Change During Growth and Are Differentially Affected by the Absence of Hfq, ProQ, or Both

- (A) WT (GSO982), *Δhfq* (GSO954), *ΔproQ* (GSO956), and *Δhfq ΔproQ* (GSO957) cells were grown for indicated times after dilution of the overnight culture, and total RNA was analyzed as in Figure 1D.
- (B) Comparison between RNA levels in WT (GSO982) and *ΔproQ* (GSO956) (from Table S4). Red dots indicate RNAs that increase or decrease by ≥ 2 -fold. Among these, *ompC* is induced ~ 2 -fold and *ompF* is decreased ~ 4 -fold in the *ΔproQ* strain. Three biological repeats of WT (GSO982) and *ΔproQ* (GSO956) were grown to OD₆₀₀ ~1.0; total RNA was extracted and used for the construction of cDNA libraries, which were analyzed as described in STAR Methods.
- (C) The same RNA isolated for the WT (GSO982), *Δhfq* (GSO954), *ΔproQ* (GSO956), and *Δhfq ΔproQ* (GSO957) cells in (A) was separated on an agarose gel and subjected to northern analysis using oligonucleotides specific to the 5' ends of *ompC*, *ompF*, and 5S RNA sequentially on the same membrane.
- (D) The blot for WT (GSO982), *Δhfq* (GSO954), *ΔproQ* (GSO956), and *Δhfq ΔproQ* (GSO957) samples in (A) was probed with an oligonucleotide specific to the 3' end of *hupB*. The *hupB* 3' panel corresponds to a longer exposure of the *hupB* blot.
- (E) WT (GSO982), *ΔproQ* (GSO958), *Δmb* (GSO968), and *ΔproQ Δmb* (GSO964) cells were grown for 150 min after dilution of the overnight culture. Total RNA separated on an acrylamide gel was subjected to northern analysis and sequentially probed with oligonucleotides specific to the 3' ends of the *cspE*, *hupB*, and *ompC* RNAs. The bottom *cspE* and *hupB* panels corresponded to longer exposures of the corresponding top panels. The same total RNA was also separated on an agarose gel and subjected to northern analysis using the *ompC* oligonucleotide. Both blots were also probed for the 5S RNA (Figure S2D).

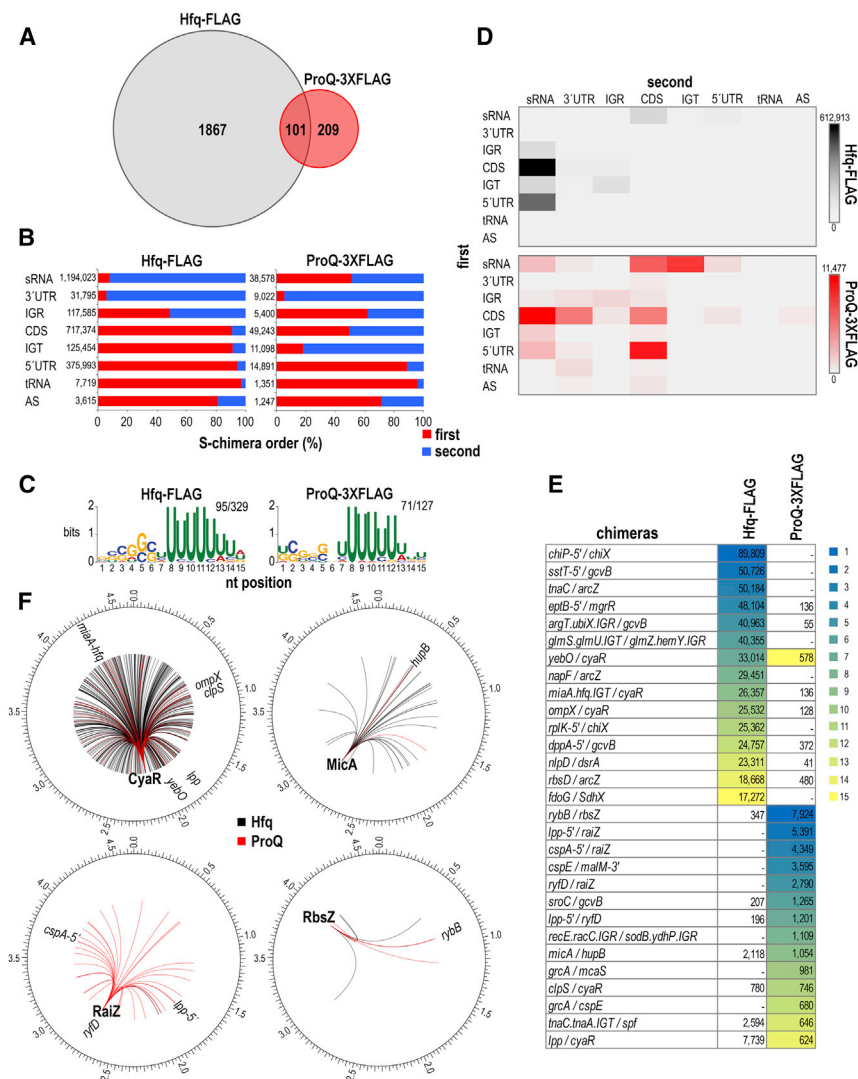


Figure 3. Most RNA Pairs Differ Between Hfq- and ProQ-Bound Chimeras

(A) Venn diagram showing ~33% of the RNA pairs found on ProQ-3XFLAG are shared with Hfq-FLAG for samples grown in LB. Only chimeras with unique names were counted.

(B) Distribution of RNA locations as first (red) and second (blue) in chimera fragments for RNAs derived from various genomic elements in Hfq LB and ProQ LB datasets.

(C) Motifs found for second RNA in Hfq LB ($E = 1.8 \times 10^{-55}$) and ProQ LB ($E = 1.5 \times 10^{-27}$) datasets. Fractions correspond to number of sequences containing motif, over the total number analyzed.

(D) Total number of chimeric fragments for each combination of genomic elements in the Hfq LB and ProQ LB datasets. Rows represent the first RNA in the chimera, and columns represent the second RNA in the chimera. The most prominent pairs in the Hfq dataset are sRNAs as the second RNA with CDS or 5'UTRs as the first RNA, whereas other combinations are also abundant in the ProQ dataset.

(E) The top 15 chimeras in Hfq LB and ProQ LB datasets, with the exception of *yebO*-CyaR, are different, however, some chimeras are found at lower levels for both proteins. The enrichment value is given with the boxes for the top 15 most-enriched RNAs shaded according to the key.

(F) Each sRNA has a unique pattern of partner RNAs. While almost all chimeras for RaiZ are found on ProQ, most chimeras for MicA are found on Hfq, with a few found on ProQ. RbsZ, the sRNA comprising half of the top chimera in ProQ dataset, is only present in a limited number of chimeras. Circos plots were drawn by circos software (<http://circos.ca>).

For (B) and (D), mapped fragments were classified as in Figure 1A.

and impacting the levels of 3' UTR fragments via a mechanism that is independent of RNase II and different from the mechanism by which ProQ affects full-length mRNAs. The role ProQ plays in generating or stabilizing these fragments deserves more investigation. However, we next turned to the RNA chimeras detected for Hfq and ProQ.

Several RNA Pairs Associate with Both Hfq and ProQ

To gain a better statistical power with the RIL-seq datasets, we combined the mapped chimeric fragments of all libraries in each condition to a unified dataset as described previously (Melamed et al., 2016). The percentage of chimeric fragments out of the total number of mapped fragments was similar for both Hfq and ProQ datasets (9%–12%) (Table S1). For these combined libraries, we only considered statistically significant chimeric fragments (S-chimeras as defined in Melamed et al., 2016). Since some S-chimeras were detected in the negative control libraries (*E. coli* with untagged Hfq and ProQ), we calculated an additional threshold that eliminated 90% of the S-chimeras in the control

libraries (see STAR Methods and Figure S3A for details). Thus, we only considered unique interactions supported by at least 39 chimeric fragments for cells grown in LB and at least 60 chimeric fragments for cells grown in M63. Computed hybridization-free energies for RNA pairs that did not pass the statistical filtering were higher than for RNA pairs included in the final datasets (Figure S3B) supporting this threshold. The filtered datasets were used for further analysis.

There were more chimeras for Hfq than for ProQ; 1,968 versus 310 for LB-grown cells and 1,067 versus 33 for M63-grown cells (Figures 3A and S3C). The reason for the dramatically lower number of chimeras for ProQ in M63-grown cells is not known, though most chimeras detected in M63-grown cells are also found in LB-grown cells (Table S5).

Interestingly, 33% of the chimeras for ProQ were also found on Hfq in LB-grown cells (Figure 3A). Among this overlap set, DAVID functional annotation analysis (Table S5) revealed that there was enrichment for a cluster comprised of outer membrane proteins and porins. We noted several RNAs that were strongly enriched

by binding to ProQ, such as *ryfA*, *ibsA*, and *infA* (Figure 1C), were not found in the most abundant chimeras. The second RNA in Hfq-dependent chimeras tends to be an sRNA (Figures 3B and S3D) as has been reported previously, likely due to preferential sRNA-binding to the proximal face of Hfq (Melamed et al., 2016). For ProQ-dependent chimeras in contrast, known sRNAs were either first or second, while 3' UTRs were more prevalent as the second RNA. For both Hfq and ProQ, the second RNAs, but not the first RNAs, were enriched for a GC-rich sequence followed by polyU stretch, the elements of intrinsic terminators (Figures 3C and S3E). As expected, for Hfq the most abundant RNA pairs were between the 5' UTR or CDS of mRNAs and sRNAs (Figures 3D and S3F). The pairs were much more varied in the ProQ datasets. RNA pairs between sRNAs and the 5' UTR or CDS of mRNAs were observed, but other RNA pairs were also highly abundant possibly reflecting multiple, different ProQ roles.

Among the 15 top chimeras found on each protein (Figures 3E and S3G), most are different between Hfq and ProQ, although the well-characterized Hfq-binding sRNAs RybB, GcvB, MicA, McaS, CyaR, and Spot 42 are part of the top 15 chimeras on ProQ in LB. Several of the top chimeras detected for Hfq such as *chiP*-ChiX and *eptB*-MgrR correspond to well-characterized mRNA-sRNA interactions (Figuroa-Bossi et al., 2009; Moon and Gottesman, 2009; Rasmussen et al., 2009). The chimeras detected for ProQ, such as *lpp*-RaiZ, *MicA*-*hupB*, and *grcA*-McaS could correspond to uncharacterized sRNA-mRNA regulatory pairs. Other abundant ProQ-bound pairs, such as RybB-RbsZ, and RyfD-RaiZ are comprised of two sRNAs.

Comparisons between the target sets for different sRNAs revealed unique patterns that can be visualized by the Circos plots in Figure 3F. The chimeras with RaiZ were detected almost exclusively in the ProQ dataset (red lines). In contrast, MicA chimeras were predominant in the Hfq dataset (gray lines), though some chimeras also were found associated with ProQ. The numbers of detected chimeras also varied widely, with only a few for RbsZ but large numbers for CyaR. These analyses indicate that while Hfq and ProQ bind overlapping sets of RNA pairs, there are differences between the two proteins, likely reflecting differences in function.

Chimera Formation Is Not Dependent on the Second RNA Chaperone

The observation that 33% of the chimeras found on ProQ are also associated with Hfq led to the question of whether the two proteins are found in the same complex. To test this, we carried out reciprocal co-purification experiments in which we determined the levels of ProQ that co-purify with Hfq-FLAG and the levels of Hfq that co-purify with ProQ-3XFLAG. Given the varied effects of the Δhfq and $\Delta proQ$ deletions on sRNA and mRNA levels across growth, we examined Hfq and ProQ levels at different time points in LB and minimal glucose media (Figures 4A and S4A) and assayed co-purification at 150 and 360 min of growth in LB (Figures 4B and S4B). Hfq and ProQ levels change somewhat over the time, with some differences between rich and minimal media for ProQ. However, no ProQ was found to directly co-purify with Hfq-FLAG at either condition tested. A small amount of Hfq co-purified with

ProQ-3XFLAG, but this is likely due to binding of the same RNA because the co-purification was abolished when the extracts were treated with RNase.

Another explanation for the chimeras found in both the Hfq and ProQ datasets is that RNA pairs chaperoned by Hfq are subsequently bound by ProQ or vice versa. This possibility was explored by repeating the RIL-seq experiments for ProQ-3XFLAG cells lacking Hfq and for Hfq-FLAG cells lacking ProQ grown to the 150 min time point (Tables S6 and S7, Figure S4C). Top chimeras for this second RIL-seq experiment (2) were compared to the top chimeras for the first RIL-seq experiment (1) (Figures 4C and 4D). Although the samples were obtained from cells grown under slightly different conditions, OD₆₀₀ ~10 compared to 150 min (OD₆₀₀ ~14 in the WT background), there is substantial overlap between the top chimeras. Many of the top chimeras observed in the WT background are also top chimeras in both deletion back-grounds (Figures 4C and 4D; Table S7). Even for chimeras no longer ranked among the top 10 in Δhfq and $\Delta proQ$, we still observe many chimeras. One exception for which very few chi-meras were observed with ProQ-3XFLAG in the Δhfq background is *grcA*-McaS. These low levels may reflect the fact that McaS has been categorized as a Class II Hfq binding sRNA whose levels are particularly sensitive to the absence of Hfq (Schu et al., 2015). Overall, the finding that the top chimeras are similar between the WT and $\Delta proQ$ backgrounds for Hfq-FLAG as well as WT and Δhfq backgrounds for ProQ-3XFLAG indicated that the RNAs are in proximity and therefore likely pair on the two RNA-binding proteins independent of the other chaperone.

Hfq and ProQ Differentially Impact RbsZ Downregulation of RybB

To better understand the physiological role of the chimeras found on both proteins, we next investigated the consequences of the interactions with Hfq and ProQ for the chimera comprised of the RybB and RbsZ sRNAs. The RybB-RbsZ pair was the most abundant chimera found on ProQ in the two independent LB datasets in both orientations (RybB-RbsZ and RbsZ-RybB) but was also present on Hfq, though at lower numbers in only one orientation (RybB-RbsZ) (Figures 3E, 4D, and 5A). The σ^E -dependent RybB sRNA, which has been characterized extensively in both *E. coli* and *S. enterica*, represses the synthesis of a number of outer membrane proteins including OmpC (Gogol et al., 2011; Papenfort et al., 2006; Thompson et al., 2007). The RybB chimeras with RbsZ map to the *rbsB*-*rbsK* intergenic region of the ribose catabolism operon (Figure 5A). Closer inspection of the transcripts in this region suggested that a promoter internal to the *rbsB* gene drives synthesis of the ~200 nt RbsZ sRNA (Thomason et al., 2015). Under some conditions, this transcript is cleaved to shorter forms (collectively denoted RbsZ-S). RbsZ-S, but not RbsZ levels, are elevated for cells grown in minimal M63 medium with ribose (Figure S5A). Thus, it is likely that RbsZ-S is derived from RbsZ as well as from the mRNAs encoding *rbsDACB* and *rbsB*, which also has its own promoter (Thomason et al., 2015). While RbsZ and RbsZ-S both are bound by Hfq and ProQ, IP enrichment for RbsZ is stronger with ProQ and IP enrichment for one form of RbsZ-S is stronger with Hfq (Figure 1D; Table S2).

Given that the levels of RbsZ do not decrease in a Δhfq background (Figure 2A) and very few RNAs were partnered with this

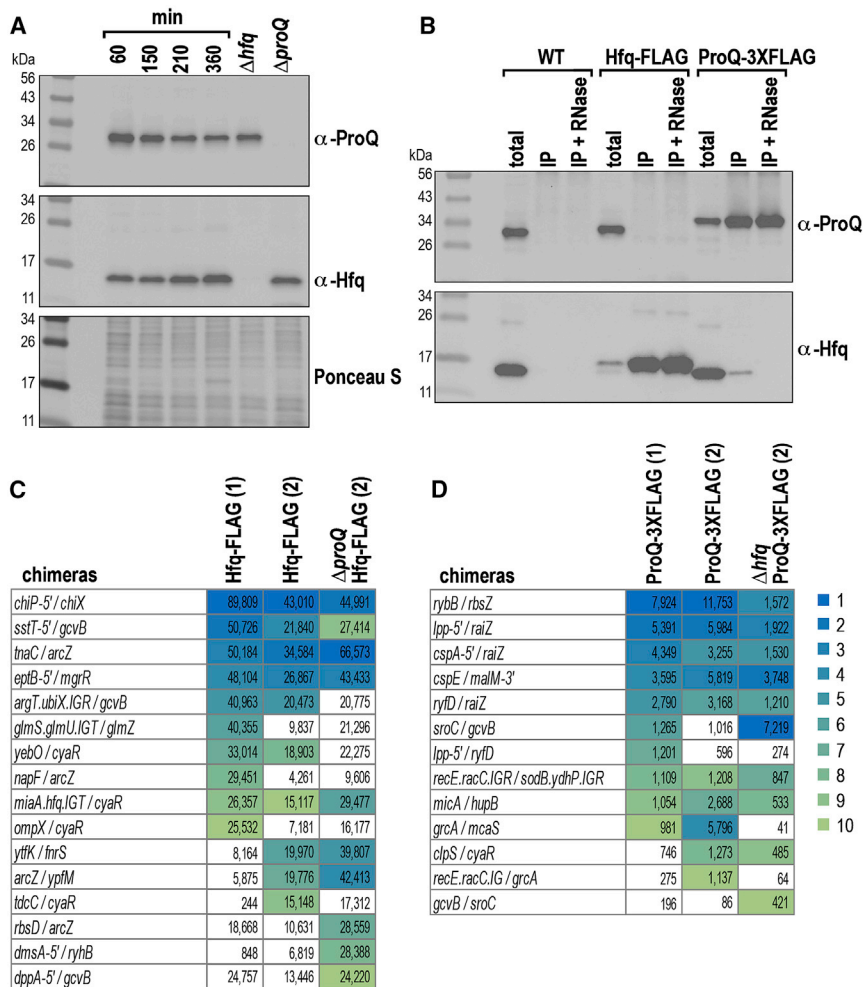


Figure 4. ProQ Promotes RNA Interactions Independently of Hfq

(A) Relative levels of ProQ and Hfq for time points assayed in Figure 2 were determined by immunoblot analysis using α -ProQ or α -Hfq antibodies.

(B) Immunoblot analyses using α -ProQ or α -Hfq antibodies of immunoprecipitated Hfq-FLAG (HM34) or ProQ-3XFLAG (GSO953) for samples taken at 150 min. Indicated IP samples were also subjected to treatment with a mix of RNase A and RNase T1.

(C) Comparison of the top chimeras in RIL-seq experiment 1 from WT Hfq-FLAG (HM34) in Figure 3 and in RIL-seq experiment 2 from WT Hfq-FLAG (HM34) and Δ proQ Hfq-FLAG (GSO969) cells harboring Hfq-FLAG.

(D) Comparison of the top chimeras in RIL-seq experiment 1 from WT ProQ-3XFLAG (GSO953) in Figure 3 and in RIL-seq experiment 2 from ProQ-3XFLAG (GSO953) and Δ hfq ProQ-3XFLAG (GSO960) cells harboring ProQ-3XFLAG.

For both (C) and (D), the enrichment value is given with the boxes for the top 10 most-enriched RNAs shaded according to the key.

(Johansen et al., 2006), for the same RNA samples (Figure 5B). Again, different effects of Δ hfq and Δ proQ are observed at 150 and 360 min. At 150 min, we observed an overall increase in *ompC* mRNA levels in the Δ proQ strains (lanes 5 and 6) as in Figure 2C. This effect of ProQ is not detected at 360 min (lanes 13 and 14), possibly due to higher RybB levels. Instead, there is a Δ hfq-dependent increase (lanes 11 and 12). In addition, *ompC* mRNA levels are elevated in both the WT and Δ proQ strains

transcript (Figure 3F), we hypothesized that RbsZ might be acting as a sponge to downregulate RybB. We thus examined the consequences of RbsZ overexpression in exponential and stationary phase (150 and 360 min after subculturing) in a WT background (Figure 5B). Consistent with our hypothesis, RybB levels were significantly reduced in the pBR-RbsZ cells at both time points (lane 2 versus 1, lane 10 versus 9), with a more striking effect at 360 min (lane 10), when endogenous RybB levels are highest (Figure 2A). RybB levels also were reduced upon just RbsZ-S overexpression at 360 min (Figure S5B). Accordingly, RybB levels increased in cells lacking RbsZ or RbsZ-S (Figure S5C). We also collected samples from Δ hfq, Δ proQ, and Δ hfq Δ proQ mutant strains at the same 150 and 360 time points (Figure 5B). At the later time point, RybB levels are very low in the Δ hfq mutant cells, and no further reduction is observed with RbsZ overexpression (lane 12 versus 11), though as was also seen in Figure 2A, new slower-migrating bands are seen in the Δ hfq background. In contrast, RybB levels overall were higher in the Δ proQ strain with RbsZ-dependent repression that was similar to that in WT cells (lane 14 versus 13).

We also assessed the consequences of RbsZ overexpression on the levels of the *ompC* mRNA, a verified *E. coli* RybB target

when RbsZ is overexpressed (lane 10 versus 9, lane 14 versus 13, respectively). This RbsZ-dependent increase in *ompC* levels was eliminated in a Δ rybB strain background (Figure 5C), suggesting that the effect of RbsZ on *ompC* is through RybB. Together these results indicate that RbsZ is acting as a sponge to lower RybB levels and this is dependent on Hfq.

To test the predicted base pairing between RybB and RbsZ (Figure 5D), which overlaps the well-defined seed or base pairing region of RybB (Papenfert et al., 2010) and is contained in RbsZ-S, we generated two RbsZ mutants. In the WT background, the RbsZ-M2 mutation eliminated RbsZ-dependent reduction of RybB (Figure 5E). Interestingly, the RbsZ-M1 mutation resulted in elevated levels of RybB. This RybB induction is not due to activation of the cell envelope response, because the levels of another σ^E -dependent sRNA, MicA, were not increased in the RbsZ-M1 mutant strains. We suggest that RbsZ-M1 still binds to the critical 5' end of the RybB seed sequence and blocks degradation in this configuration. Compensatory mutations in the chromosomally encoded copy of *rybB* had similar effects. Consistent with the predicted base pairing, RybB-M1 levels were reduced in the pBR-RbsZ-M1 background and increased in the pBR-RbsZ background. RybB-M2 levels overall

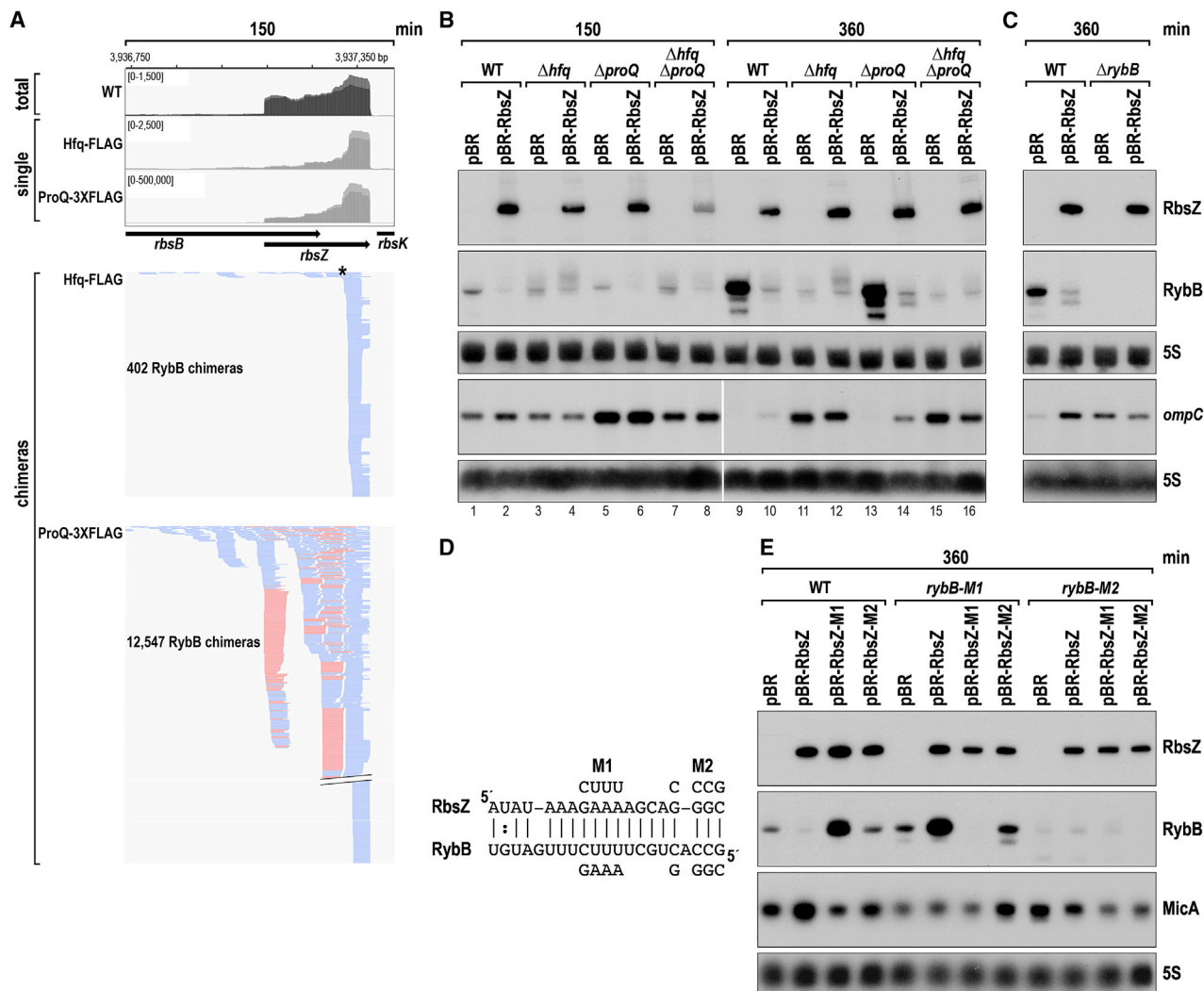


Figure 5. RbsZ Sponges RybB, Inducing OmpC Levels

(A) Browser image showing RybB chimeras at *rbsZ* locus. Data are from Hfq-FLAG and ProQ-3XFLAG LB RIL-seq experiment 2. Top: signals for total RNA (dark gray) and RIL-seq single fragments with two biological repeats are overlaid (light gray). Read count ranges are shown in the upper left of each frame. Bottom: chimeras with RybB in unified datasets. Red and blue lines indicate RbsZ is first or second RNA in the chimera, respectively. The numbers differ from the number in Figure 3D because they include RNA pairs in both orientations. Asterisk indicates position of RbsZ-RybB base pairing.

(B) RybB levels decrease in the presence of RbsZ. Total RNA was extracted from WT (GSO982), Δhfq (GSO955), $\Delta proQ$ (GSO956), and $\Delta hfq \Delta proQ$ (GSO959) strains harboring the indicated plasmids 150 and 360 min after dilution of the overnight culture.

(C) RbsZ affects *ompC* levels in an RybB-dependent manner. Total RNA was extracted from WT (GSO982) and $\Delta rybB$ (GSO970) strains harboring the indicated plasmids 360 min after dilution of the overnight culture.

(D) Base pairing between RbsZ and RybB with sequences of mutants generated.

(E) Test of direct interaction between RbsZ and RybB. Total RNA was extracted from WT (GSO982), *rybB-M1* (GSO961), and *rybB-M2* (GSO962) strains harboring the indicated plasmids 360 min after dilution of the overnight culture.

For (B), (C), and (E), total RNA was either separated an acrylamide gel, transferred to a membrane, and sequentially probed for the RybB, RbsZ and 5S RNAs or separated on an agarose gel, transferred to a membrane, and sequentially probed for the *ompC* and 5S RNAs. Due to the large number of samples in (B), the total RNA was run on two different parts of an agarose gel.

were lower for unknown reasons but were decreased only by pBR-RbsZ-M2. These phenotypes are consistent with RybB-RbsZ base pairing through the predicted region.

RybB-*rbsB*-RbsZ Form an Autoregulatory Loop

RbsZ corresponds to the 3' UTR of *rbsB*, which encodes a periplasmic ribose binding protein required for ribose uptake

and which impacts chemotaxis toward ribose (Galloway and Furlong, 1977). We noticed that there are also Hfq- and ProQ-dependent chimeras between RybB and the 5' end of *rbsB* (Figure 6A and Table S7). There were similar numbers of RybB-*rbsB* chimeras on Hfq and ProQ (Figure 6A). Most of the chimeras on ProQ are found slightly downstream of the *rbsB* start codon. In contrast, the chimeras on Hfq are

ProQ, indicating a RybB-*rbsB* interaction can take place independent of the two RNA chaperones. To test whether the base pairing previously predicted for RybB-*rbsB* (Gogol et al., 2011) (Figure 6D) is responsible for the repression, we constructed *gfp* fusions to WT and M2 mutant versions of *rbsB*. Consistent with the predicted pairing, RybB reduced expression from *rbsB-gfp* but not *rbsB-M2:gfp*, while RybB-M2 did not regulate *rbsB-gfp* but did repress *rbsB-M2-gfp* (Figure 6E).

ProQ Protects RybB from RbsZ-, Hfq-, and RNase III-Dependent Downregulation

We noted that while we detected more RybB-RbsZ chimeras associated with ProQ than Hfq for cells grown in LB medium (Figure 5A), RbsZ downregulation of RybB was still observed in a Δ *proQ* mutant (Figure 5B). These observations indicate that ProQ binding to the RybB-RbsZ pair might have consequences different from Hfq binding. We considered the possibility that ProQ sequesters and protects the RybB-RbsZ hybrid from the RybB downregulation seen in the presence of Hfq and wondered whether higher levels of ProQ would further block this downregulation. To test this possibility, we overexpressed ProQ from a plasmid in the Δ *proQ* background with or without concomitant RbsZ overexpression (Figure 7A). Northern analysis showed that, indeed, higher levels of ProQ prevented downregulation by RbsZ, even though RbsZ levels were higher in this strain. In fact, with ProQ overexpression, RbsZ increased RybB levels similar to what was observed with the RbsZ-M1 or RybB-M1 mutants (Figure 5E). Intriguingly, whole transcriptome analysis revealed that ProQ pulse overexpression for 30 min globally increased the levels of many transcripts, particularly 3' UTR RNAs (Figure 7B; Table S8). We suggest these observations can explain the different numbers of ProQ- and Hfq-associated chimeras. The protective interaction of ProQ with RybB-RbsZ is stable, resulting in higher numbers of chimeras, while the interaction on Hfq is transient, persisting only until RybB is degraded.

The higher RybB levels observed with the ProQ overproduction and the M1 mutants suggested that the RybB sRNA was being degraded in a RbsZ-dependent manner. To determine which RNase was involved in this degradation, we next examined RybB levels in various RNase mutant strains upon RbsZ overproduction (Figure 7C). We still observed downregulation in strains lacking RNase II and the other 3'-5' exoribonucleases, RNase R and PNPase, as well as in a strain in which RNase E, the endoribonuclease involved in the degradation of many sRNA-target pairs (Massé et al., 2003), was inactivated. In contrast, the RbsZ effect was abolished in the strain lacking RNase III. We suggest that the long double-stranded region of RybB-RbsZ is a target of this double-stranded RNA-specific endoribonuclease, but this cleavage can be blocked by ProQ binding. M1 mutations, in either RybB or RbsZ, also block cleavage by eliminating the formation of the appropriate double-stranded RNase III substrate. This effect of base pairing on RNase III-mediated cleavage can be recapitulated with purified components *in vitro* (Figure 7D), where base pairing between the two WT RNAs or two M1 mutant RNAs leads to RNase III cleavage in the region of pairing, which is not observed if only one of the RNAs has the mutant sequence.

Together our results for just the *rbsB* region of the chromosome illustrate how the consequences of Hfq and ProQ binding

can vary for different transcripts; the effects can be antagonistic as for RbsZ-RybB sRNA or neutral as for RybB-*rbsB* (Figure 7E). We suggest that these combinatorial effects allow for optimal control in sRNA-mediated regulation.

DISCUSSION

Collectively, this work expands the global identification of base pairing sRNA targets within *E. coli* and provides insights into shared and divergent roles of the Hfq and ProQ RNA chaperones. These results show that the base pairing sRNA network is even more nuanced than previously imagined.

RIL-Seq Can Be Applied to Divergent RNA-Binding Proteins

Our study demonstrates that the RIL-seq approach can be applied to RNA-binding proteins other than Hfq. The initial application of RIL-seq to Hfq in *E. coli* expanded the RNA-RNA network by an order of magnitude to ~2,800 interactions (Melamed et al., 2016). Since this report, several interactions on Hfq detected by RIL-seq were shown to be relevant to various biological pathways and the sequences of the chimeric fragments found to be predictive of the base pairing interactions (De Mets et al., 2019; Hoekzema et al., 2019; Miyakoshi et al., 2019; Yin et al., 2019), confirming the robustness of the approach. While the RNA-RNA network associated with Hfq already was extensively studied, only two RNA-RNA interactions, RaiZ-*hupA* and STnc540-*mgfB*, were previously reported to be facilitated by ProQ in *S. enterica* (Smirnov et al., 2017b; Westermann et al., 2019). Our study reveals hundreds of RNA pairs are found on ProQ, which can now be studied in more detail. The work also points to a broader application of the RIL-seq approach to other proteins, different mutant backgrounds, and likely mutant derivatives of these RNA-binding proteins.

As is the case for all methodologies, some cautions should be noted. The chimeras indicate that the two corresponding RNAs are found in proximity to each other on Hfq or ProQ but do not confirm that the proteins are promoting base pairing. While this is likely the case for most chimeras on Hfq, this may not be true for all chimeras on ProQ. We could document base pairing for the RybB-RbsZ chimera examined in more detail, but it is possible that the base pairing took place prior to binding ProQ. Additionally, the number of chimeras may not correlate with the strength of the regulation and can be affected by the outcome of the regulation, such as changes in RNA stability. We suggest that a difference in outcome, the promotion of RybB degradation on Hfq compared to the protection against degradation on ProQ, provides an explanation for the different number of RybB-RbsZ chimeras on the two proteins. We also noted that only a limited number of different chimeras were detected for some sRNAs such as RybB, despite the fact that multiple mRNA targets have been reported (Gogol et al., 2011). The very 5' end of RybB has been shown to be involved in base pairing with targets. It is possible that this type of pairing may constrain the number of chimeras that can be captured by RIL-seq. Nevertheless, the current study provides a wealth of information for future analyses (see STAR Methods for links to interactive browsers).

Growth Conditions Impact Effect of sRNAs and RNA Chaperones

Our work also illustrates that growth phase impacts the ability of an RNA-binding protein and an sRNA to regulate an mRNA. This likely is due to multiple factors including, but not limited to, the relative levels of the mRNA, sRNA, Hfq, and ProQ as well as the levels of competing RNA chaperones, RNases, sRNAs, mRNAs, and sRNA sponges. The effects of $\Delta proQ$, Δhfq , the RybB sRNA, and the RbsZ sponge on *ompC* mRNA levels at 150 and 360 min of growth clearly illustrate this point (Figures 2C and 5B). While $\Delta proQ$ leads to overall higher levels of the mRNA at 150 min, regulation by RybB is more strongly affected by Δhfq at 360 min. It is also interesting to note that while a comparable number of chimeras were detected on Hfq in LB and in M63, the number of chimeras detected on ProQ was significantly smaller in M63 compared to LB, emphasizing the influence of media on the roles of the RNA chaperones. Growth conditions should be considered in future studies of sRNA-mediated regulation and ProQ.

Given the reported role of ProQ in osmoprotection, we noted that the levels of a number of mRNAs, like *ompC*, whose levels were most strongly affected by the lack of ProQ and which were found in the top ProQ bound chimeras, encode gene products critical for the *E. coli* response to osmotic stress. We suggest that the decreased resistance to osmotic stress observed for the $\Delta proQ$ mutant strain (Kerr et al., 2014) may in part be due to OmpR-independent effects on *ompC*, *ompF*, and *OmrA* as well as altered sRNA-mediated regulation. The influence of Hfq or ProQ may be different under specific stress conditions such as osmotic stress.

ProQ and Hfq Have Different Roles, Allowing Nuanced Regulation

ProQ was proposed to play a similar role to Hfq in bacteria, as it was found to be the matchmaker of the RaiZ sRNA-*hupA* mRNA interaction (Smirnov et al., 2017b), and other FinO-domain proteins also promote sRNA-mRNA pairing (Attaiech et al., 2016; Chaulk et al., 2011). However, our data indicate that this may not be true for all RNAs bound by ProQ. One difference from Hfq, which binds sRNAs and mRNAs equally, is that ProQ predominantly binds mRNAs (Figure 1A). Additionally, the order of the RNAs and the types of RNAs in the chimeric fragments is more varied on ProQ than on Hfq. Finally, while many of the top bound sRNAs and mRNAs on Hfq are found in the top chimeras, this is only partially true for ProQ, though the chimera dataset overall was significantly smaller.

Our findings also suggest that, while Hfq is involved primarily in sRNA-mediated regulation of mRNA translation, ProQ may have multiple roles in the cell, with RNA-RNA matchmaking possibly being a minor role. Recent work showed ProQ protects the *cspE* mRNA from degradation by RNase II (Holmqvist et al., 2018). We also observe some protective effect on the *cspE* mRNA but detected a ProQ-dependent protection of 3' UTR fragments not impacted by RNase II. Additionally, our findings suggest that ProQ is in competition with Hfq on some of the RNA pairs, blocking Hfq-mediated regulation. Moreover, given the different consequences of $\Delta proQ$ for the levels of full-length mRNAs compared to 3' fragments of these mRNAs, it is possible that

ProQ has different roles for different portions of an RNA transcript. The preferential binding of ProQ internal to coding sequences raises the question of whether the protein impacts other aspects of the RNA life cycle such as modification. Taken together, the ProQ role and mode of action differ from those of the well-studied Hfq protein, with many aspects needing further exploration.

While the paradigm of one gene to one RNA or protein was accepted for many years, it is becoming increasingly evident that a single genomic region can encode multiple functional products (Meydan et al., 2019; Miyakoshi et al., 2015; Weaver et al., 2019). The small genomic region encompassing *rbsB*, which is a focus of this study, illustrates how multiple functional transcripts can be derived from a single genomic region. For the RybB-*rbsB*-RbsZ example we explored here, this results in an autoregulatory loop (Figure 7E). We suggest that when *rbsB* and consequently RbsZ-S levels are induced, RbsZ-S sponges RybB and prevents *rbsB* downregulation, thus accentuating *rbsB* induction. Conversely, when RybB levels increase above those of RbsZ, RybB downregulates *rbsB*, which in turn might lead to reduced RbsZ-S levels and therefore increased active RybB, amplifying the negative regulation. The physiological role of this crosstalk between the ribose regulon and a σ^E -dependent sRNA deserves further study. Perhaps the *rbsACB*-encoded transporter renders cells particularly vulnerable to cell envelope stress, but is critical, despite stress, when only the poor carbon source ribose is available.

The RIL-seq analysis indicates that similar complexity exists for multiple genes. In general, this study uncovered how much remains to be learned about the sRNA regulatory network of the well-studied model *E. coli*, implying we have only scratched the surface for other bacteria.

STAR★METHODS

Detailed methods are provided in the online version of this paper and include the following:

- KEY RESOURCES TABLE
- LEAD CONTACT AND MATERIALS AVAILABILITY
- EXPERIMENTAL MODEL AND SUBJECT DETAILS
 - Bacteria
- METHOD DETAILS
 - Plasmid construction
 - RNA isolation
 - RIL-seq
 - RNA-seq
 - RNA coimmunoprecipitation (Co-IP) assay
 - Protein coimmunoprecipitation (Co-IP) assay
 - Northern blot analysis
 - Immunoblot analysis
 - RNA structure probing
 - GFP reporter assay
- QUANTIFICATION AND STATISTICAL ANALYSIS
 - Spearman correlation between libraries
 - RNA enrichment in RIL-seq libraries
 - Cutoffs for chimeras in RIL-seq libraries
 - Venn diagrams
 - Circos plots

- Browser images
- Free energy of hybridization calculations
- Recognition of sequence motifs
- Functional annotation analysis
- **DATA AND CODE AVAILABILITY**
 - Chimeras
 - Coverage
 - IP and total
 - Annotations
 - Pairs
 - Mendely Data

SUPPLEMENTAL INFORMATION

Supplemental Information can be found online at <https://doi.org/10.1016/j.molcel.2019.10.022>.

ACKNOWLEDGMENTS

We thank members of the group of Hanah Margalit for sending the Hfq-FLAG strain and assistance with the computational analysis, particularly Asaf Peer for help with the RIL-seq software. We thank the NICHD Molecular Genomics Core, particularly Tianwei Li, for all of the library sequencing and the NICHD Bioinformatics and Scientific Programming Core, particularly Ryan Dale and Sydney Hertafeld, for setting up the browsers. We are grateful to the Storz lab for all of the helpful discussions and comments on the manuscript. We also appreciate the comments from Susan Gottesman, Hanah Margalit, Kai Papenfort, and Mikolaj Olejniczak. This work was supported by the Intramural Research Program of the Eunice Kennedy Shriver National Institute of Child Health and Human Development. This work is dedicated to the memory of Jacob Abiry who had the curiosity and the ambition to learn new things every day.

AUTHOR CONTRIBUTIONS

S.M. and G.S. conceived of the project. S.M., P.P.A., and A.Z. designed, performed, and analyzed all experiments. H.Z. performed all the computational analyses under the supervision of S.M. S.M., P.A., A.Z., H.Z., and G.S. prepared the figures and wrote the manuscript. G.S. supervised the project.

DECLARATION OF INTERESTS

The authors declare no competing interests.

Received: June 20, 2019

Revised: September 9, 2019

Accepted: October 15, 2019

Published: November 21, 2019

REFERENCES

- Adams, P.P., Flores Avile, C., Popitsch, N., Bilusic, I., Schroeder, R., Lybecker, M., and Jewett, M.W. (2017). In vivo expression technology and 5' end mapping of the *Borrelia burgdorferi* transcriptome identify novel RNAs expressed during mammalian infection. *Nucleic Acids Res.* **45**, 775–792.
- Attaiech, L., Boughammoura, A., Brochier-Armanet, C., Allatif, O., Peillard-Fiorente, F., Edwards, R.A., Omar, A.R., MacMillan, A.M., Glover, M., and Charpentier, X. (2016). Silencing of natural transformation by an RNA chaperone and a multitarget small RNA. *Proc. Natl. Acad. Sci. USA* **113**, 8813–8818.
- Baba, T., Ara, T., Hasegawa, M., Takai, Y., Okumura, Y., Baba, M., Datsenko, K.A., Tomita, M., Wanner, B.L., and Mori, H. (2006). Construction of *Escherichia coli* K-12 in-frame, single-gene knockout mutants: the Keio collection. *Mol Syst Biol.* **2**, 2006.0008.
- Bailey, T.L., Boden, M., Buske, F.A., Frith, M., Grant, C.E., Clementi, L., Ren, J., Li, W.W., and Noble, W.S. (2009). MEME SUITE: tools for motif discovery and searching. *Nucleic Acids Res.* **37**, W202–208.
- Cech, T.R., and Steitz, J.A. (2014). The noncoding RNA revolution—trashing old rules to forge new ones. *Cell* **157**, 77–94.
- Chaulk, S.G., Smith Frieday, M.N., Arthur, D.C., Culham, D.E., Edwards, R.A., Soo, P., Frost, L.S., Keates, R.A., Glover, J.N., and Wood, J.M. (2011). ProQ is an RNA chaperone that controls ProP levels in *Escherichia coli*. *Biochemistry* **50**, 3095–3106.
- Chen, H., and Boutros, P.C. (2011). VennDiagram: a package for the generation of highly-customizable Venn and Euler diagrams in R. *BMC Bioinformatics* **12**, 35.
- Cherepanov, P.P., and Wackernagel, W. (1995). Gene disruption in *Escherichia coli*: TcR and KmR cassettes with the option of Flp-catalyzed excision of the antibiotic-resistance determinant. *Gene* **158**, 9–14.
- Coornaert, A., Lu, A., Mandin, P., Springer, M., Gottesman, S., and Guillier, M. (2010). MicA sRNA links the PhoP regulon to cell envelope stress. *Mol. Microbiol.* **76**, 467–479.
- Corcoran, C.P., Podkaminski, D., Papenfort, K., Urban, J.H., Hinton, J.C., and Vogel, J. (2012). Superfolder GFP reporters validate diverse new mRNA targets of the classic porin regulator, MicF RNA. *Mol. Microbiol.* **84**, 428–445.
- Datsenko, K.A., and Wanner, B.L. (2000). One-step inactivation of chromosomal genes in *Escherichia coli* K-12 using PCR products. *Proc. Natl. Acad. Sci. USA* **97**, 6640–6645.
- De Mets, F., Van Melderen, L., and Gottesman, S. (2019). Regulation of acetate metabolism and coordination with the TCA cycle via a processed small RNA. *Proc. Natl. Acad. Sci. USA* **116**, 1043–1052.
- Figuerola-Bossi, N., Valentini, M., Malleret, L., Fiorini, F., and Bossi, L. (2009). Caught at its own game: regulatory small RNA inactivated by an inducible transcript mimicking its target. *Genes Dev.* **23**, 2004–2015.
- Galloway, D.R., and Furlong, C.E. (1977). The role of ribose-binding protein in transport and chemotaxis in *Escherichia coli* K12. *Arch. Biochem. Biophys.* **184**, 496–504.
- Gogol, E.B., Rhodius, V.A., Papenfort, K., Vogel, J., and Gross, C.A. (2011). Small RNAs endow a transcriptional activator with essential repressor functions for single-tier control of a global stress regulon. *Proc. Natl. Acad. Sci. USA* **108**, 12875–12880.
- Guillier, M., and Gottesman, S. (2006). Remodelling of the *Escherichia coli* outer membrane by two small regulatory RNAs. *Mol. Microbiol.* **59**, 231–247.
- Guzman, L.M., Belin, D., Carson, M.J., and Beckwith, J. (1995). Tight regulation, modulation, and high-level expression by vectors containing the arabinose P_{BAD} promoter. *J. Bacteriol.* **177**, 4121–4130.
- Hobbs, E.C., Astarita, J.L., and Storz, G. (2010). Small RNAs and small proteins involved in resistance to cell envelope stress and acid shock in *Escherichia coli*: analysis of a bar-coded mutant collection. *J. Bacteriol.* **192**, 59–67.
- Hoekzema, M., Romilly, C., Holmqvist, E., and Wagner, E.G.H. (2019). Hfq-dependent mRNA unfolding promotes sRNA-based inhibition of translation. *EMBO J.* **38**, e101199.
- Holmqvist, E., Li, L., Bischler, T., Barquist, L., and Vogel, J. (2018). Global maps of ProQ binding in vivo reveal target recognition via RNA structure and stability control at mRNA 3' ends. *Mol. Cell* **70**, 971–982.e6.
- Hör, J., Gorski, S.A., and Vogel, J. (2018). Bacterial RNA biology on a genome scale. *Mol. Cell* **70**, 785–799.
- Huang da, W., Sherman, B.T., and Lempicki, R.A. (2009). Systematic and integrative analysis of large gene lists using DAVID bioinformatics resources. *Nat. Protoc.* **4**, 44–57.
- Johansen, J., Rasmussen, A.A., Overgaard, M., and Valentin-Hansen, P. (2006). Conserved small non-coding RNAs that belong to the sigmaE regulon: role in down-regulation of outer membrane proteins. *J. Mol. Biol.* **364**, 1–8.
- Kerr, C.H., Culham, D.E., Marom, D., and Wood, J.M. (2014). Salinity-dependent impacts of ProQ, Prc, and Spr deficiencies on *Escherichia coli* cell structure. *J. Bacteriol.* **196**, 1286–1296.
- Keseler, I.M., Mackie, A., Peralta-Gil, M., Santos-Zavaleta, A., Gama-Castro, S., Bonavides-Martínez, C., Fulcher, C., Huerta, A.M., Kothari, A.,

- Krummenacker, M., et al. (2013). EcoCyc: fusing model organism databases with systems biology. *Nucleic Acids Res.* *41*, D605–D612.
- Kunte, H.J., Crane, R.A., Culham, D.E., Richmond, D., and Wood, J.M. (1999). Protein ProQ influences osmotic activation of compatible solute transporter ProP in *Escherichia coli* K-12. *J. Bacteriol.* *181*, 1537–1543.
- Lorenz, R., Bernhart, S.H., Höner Zu Siederdisen, C., Tafer, H., Flamm, C., Stadler, P.F., and Hofacker, I.L. (2011). ViennaRNA Package 2.0. *Algorithms Mol. Biol.* *6*, 26.
- Massé, E., Escorcía, F.E., and Gottesman, S. (2003). Coupled degradation of a small regulatory RNA and its mRNA targets in *Escherichia coli*. *Genes Dev.* *17*, 2374–2383.
- Melamed, S., Peer, A., Faigenbaum-Romm, R., Gatt, Y.E., Reiss, N., Bar, A., Altuvia, Y., Argaman, L., and Margalit, H. (2016). Global mapping of small RNA-target interactions in bacteria. *Mol. Cell* *63*, 884–897.
- Melamed, S., Faigenbaum-Romm, R., Peer, A., Reiss, N., Shechter, O., Bar, A., Altuvia, Y., Argaman, L., and Margalit, H. (2018). Mapping the small RNA interactome in bacteria using RIL-seq. *Nat. Protoc.* *13*, 1–33.
- Meydan, S., Marks, J., Klepacki, D., Sharma, V., Baranov, P.V., Firth, A.E., Margus, T., Kefi, A., Vázquez-Laslop, N., and Mankin, A.S. (2019). Retapamulin-assisted ribosome profiling reveals the alternative bacterial proteome. *Mol. Cell* *74*, 481–493.e6.
- Milner, J.L., and Wood, J.M. (1989). Insertion *proQ220:Tn5* alters regulation of proline porter II, a transporter of proline and glycine betaine in *Escherichia coli*. *J. Bacteriol.* *171*, 947–951.
- Miyakoshi, M., Chao, Y., and Vogel, J. (2015). Regulatory small RNAs from the 3' regions of bacterial mRNAs. *Curr. Opin. Microbiol.* *24*, 132–139.
- Miyakoshi, M., Matera, G., Maki, K., Sone, Y., and Vogel, J. (2019). Functional expansion of a TCA cycle operon mRNA by a 3' end-derived small RNA. *Nucleic Acids Res.* *47*, 2075–2088.
- Moon, K., and Gottesman, S. (2009). A PhoQ/P-regulated small RNA regulates sensitivity of *Escherichia coli* to antimicrobial peptides. *Mol. Microbiol.* *74*, 1314–1330.
- Olejniczak, M., and Storz, G. (2017). ProQ/FinO-domain proteins: another ubiquitous family of RNA matchmakers? *Mol. Microbiol.* *104*, 905–915.
- Papenfort, K., Pfeiffer, V., Mika, F., Lucchini, S., Hinton, J.C., and Vogel, J. (2006). SigmaE-dependent small RNAs of *Salmonella* respond to membrane stress by accelerating global omp mRNA decay. *Mol. Microbiol.* *62*, 1674–1688.
- Papenfort, K., Bouvier, M., Mika, F., Sharma, C.M., and Vogel, J. (2010). Evidence for an autonomous 5' target recognition domain in an Hfq-associated small RNA. *Proc. Natl. Acad. Sci. USA* *107*, 20435–20440.
- Rasmussen, A.A., Johansen, J., Nielsen, J.S., Overgaard, M., Kallipolitis, B., and Valentin-Hansen, P. (2009). A conserved small RNA promotes silencing of the outer membrane protein YbfM. *Mol. Microbiol.* *72*, 566–577.
- Schu, D.J., Zhang, A., Gottesman, S., and Storz, G. (2015). Alternative Hfq-sRNA interaction modes dictate alternative mRNA recognition. *EMBO J.* *34*, 2557–2573.
- Shishkin, A.A., Giannoukos, G., Kucukural, A., Ciulla, D., Busby, M., Surka, C., Chen, J., Bhattacharyya, R.P., Rudy, R.F., Patel, M.M., et al. (2015). Simultaneous generation of many RNA-seq libraries in a single reaction. *Nat. Methods* *12*, 323–325.
- Sittka, A., Lucchini, S., Papenfort, K., Sharma, C.M., Rolle, K., Binnewies, T.T., Hinton, J.C., and Vogel, J. (2008). Deep sequencing analysis of small noncoding RNA and mRNA targets of the global post-transcriptional regulator, Hfq. *PLoS Genet.* *4*, e1000163.
- Smirnov, A., Förstner, K.U., Holmqvist, E., Otto, A., Günster, R., Becher, D., Reinhardt, R., and Vogel, J. (2016). Grad-seq guides the discovery of ProQ as a major small RNA-binding protein. *Proc. Natl. Acad. Sci. USA* *113*, 11591–11596.
- Smirnov, A., Schneider, C., Hör, J., and Vogel, J. (2017a). Discovery of new RNA classes and global RNA-binding proteins. *Curr. Opin. Microbiol.* *39*, 152–160.
- Smirnov, A., Wang, C., Drewry, L.L., and Vogel, J. (2017b). Molecular mechanism of mRNA repression in *trans* by a ProQ-dependent small RNA. *EMBO J.* *36*, 1029–1045.
- Stalmach, M.E., Grothe, S., and Wood, J.M. (1983). Two proline porters in *Escherichia coli* K-12. *J. Bacteriol.* *156*, 481–486.
- Streit, S., Michalski, C.W., Erkan, M., Kleeff, J., and Friess, H. (2009). Northern blot analysis for detection and quantification of RNA in pancreatic cancer cells and tissues. *Nat. Protoc.* *4*, 37–43.
- Thomason, M.K., Bischler, T., Eisenbart, S.K., Förstner, K.U., Zhang, A., Herbig, A., Nieselt, K., Sharma, C.M., and Storz, G. (2015). Global transcriptional start site mapping using differential RNA sequencing reveals novel antisense RNAs in *Escherichia coli*. *J. Bacteriol.* *197*, 18–28.
- Thompson, K.M., Rhodius, V.A., and Gottesman, S. (2007). SigmaE regulates and is regulated by a small RNA in *Escherichia coli*. *J. Bacteriol.* *189*, 4243–4256.
- Timmis, K.N., Andrés, I., and Achtman, M. (1978). Fertility repression of F-like conjugative plasmids: physical mapping of the R6–5 *finO* and *finP* cistrons and identification of the *finO* protein. *Proc. Natl. Acad. Sci. USA* *75*, 5836–5840.
- Updegrove, T.B., Zhang, A., and Storz, G. (2016). Hfq: the flexible RNA matchmaker. *Curr. Opin. Microbiol.* *30*, 133–138.
- Urban, J.H., and Vogel, J. (2009). A green fluorescent protein (GFP)-based plasmid system to study post-transcriptional control of gene expression in vivo. *Methods Mol. Biol.* *540*, 301–319.
- Uzzau, S., Figueroa-Bossi, N., Rubino, S., and Bossi, L. (2001). Epitope tagging of chromosomal genes in *Salmonella*. *Proc. Natl. Acad. Sci. USA* *98*, 15264–15269.
- van Biesen, T., and Frost, L.S. (1994). The FinO protein of IncF plasmids binds FinP antisense RNA and its target, *traJ* mRNA, and promotes duplex formation. *Mol. Microbiol.* *14*, 427–436.
- Wagner, E.G.H., and Romby, P. (2015). Small RNAs in bacteria and archaea: who they are, what they do, and how they do it. *Adv. Genet.* *90*, 133–208.
- Weaver, J., Mohammad, F., Buskirk, A.R., and Storz, G. (2019). Identifying small proteins by ribosome profiling with stalled initiation complexes. *MBio* *10*, e02819–e02818.
- Westermann, A.J., Venturini, E., Sellin, M.E., Förstner, K.U., Hardt, W.D., and Vogel, J. (2019). The major RNA-binding protein ProQ impacts virulence gene expression in *Salmonella enterica* serovar Typhimurium. *MBio* *10*, e02504–e02518.
- Woodson, S.A., Panja, S., and Santiago-Frangos, A. (2018). Proteins that chaperone RNA regulation. *Microbiol. Spectr.* *6*, RWR-0026–RWR-2018.
- Yin, X., Wu Orr, M., Wang, H., Hobbs, E.C., Shabalina, S.A., and Storz, G. (2019). The small protein MgtS and small RNA MgrR modulate the PitA phosphate symporter to boost intracellular magnesium levels. *Mol. Microbiol.* *111*, 131–144.
- Yu, D., Ellis, H.M., Lee, E.C., Jenkins, N.A., Copeland, N.G., and Court, D.L. (2000). An efficient recombination system for chromosome engineering in *Escherichia coli*. *Proc. Natl. Acad. Sci. USA* *97*, 5978–5983.
- Zhang, A., Wassarman, K.M., Ortega, J., Steven, A.C., and Storz, G. (2002). The Sm-like Hfq protein increases OxyS RNA interaction with target mRNAs. *Mol. Cell* *9*, 11–22.
- Zhang, A., Wassarman, K.M., Rosenow, C., Tjaden, B.C., Storz, G., and Gottesman, S. (2003). Global analysis of small RNA and mRNA targets of Hfq. *Mol. Microbiol.* *50*, 1111–1124.
- Zhang, H., Meltzer, P., and Davis, S. (2013). RCircos: an R package for Circos 2D track plots. *BMC Bioinformatics* *14*, 244.

STAR★METHODS

KEY RESOURCES TABLE

REAGENT or RESOURCE	SOURCE	IDENTIFIER
Antibodies		
Rabbit polyclonal anti-Hfq	Zhang et al., 2002	N/A
Rabbit polyclonal anti-ProQ	Biosynthesis	N/A
Monoclonal anti-FLAG M2 antibody	Sigma-Aldrich	Cat#F1804; RRID: AB_262044
Bacterial and Virus Strains		
JW3368 (BW25113, $\Delta ompR::kan$)	Baba et al., 2006	N/A
JW1279 (BW25113, $\Delta rnb::kan$)	Baba et al., 2006	N/A
JW5741 (BW25113, $\Delta rnr::kan$)	Baba et al., 2006	N/A
JW5851 (BW25113, $\Delta prp::kan$)	Baba et al., 2006	N/A
EH200 (MG1655 $\Delta rybB::kan$)	Hobbs et al., 2010	GSO168
NB478 (W3110 $\Delta rmc::cat$)	Yu et al., 2000	N/A
EM1277 (EM1055 <i>rne-3071 zce-726::Tn102</i>)	Massé et al., 2003	N/A
AZ234 (MC4100 $\Delta hfq::cat-sacB$)	Zhang et al., 2013	GSO613
NM400 (MG1655, mini- λ , Cm ^R , ts)	A gift from Nadim Majdalani	N/A
SMS001 (MG1655 (<i>crI</i> ⁺))	lab stock	GSO983
SMS008 (MG1655 (<i>crI</i> ⁺), <i>hfq-FLAG</i>)	Melamed et al., 2016	HM34
AZ644 (MG1655 (<i>crI</i> ⁺), <i>proQ-3XFLAG</i>)	this study	GSO953
AZ282 (MG1655 (<i>crI</i> ⁺))	lab stock	GSO982
PA008 (MG1655 (<i>crI</i> ⁺), $\Delta hfq::cat-sacB$)	this study	GSO954
PA023 (MG1655 (<i>crI</i> ⁺), $\Delta hfq::kan$)	this study	GSO955
PA010 (MG1655 (<i>crI</i> ⁺), $\Delta proQ::kan$)	this study	GSO956
PA035 (MG1655 (<i>crI</i> ⁺), $\Delta hfq::cat-sacB \Delta proQ::kan$)	this study	GSO957
PA086 (MG1655 (<i>crI</i> ⁺), $\Delta proQ$)	this study	GSO958
PA054 (MG1655 (<i>crI</i> ⁺), $\Delta proQ \Delta hfq::kan$)	this study	GSO959
PA119 (MG1655 (<i>crI</i> ⁺), $\Delta ompR::kan$)	this study	GSO967
PA121 (MG1655 (<i>crI</i> ⁺), $\Delta proQ \Delta ompR::kan$)	this study	GSO963
PA127 (MG1655 (<i>crI</i> ⁺), $\Delta rmb::kan$)	this study	GSO968
PA129 (MG1655 (<i>crI</i> ⁺), $\Delta proQ \Delta rmb::kan$)	this study	GSO964
SMS074 (MG1655 (<i>crI</i> ⁺), $\Delta hfq::cat proQ-3XFLAG$)	this study	GSO960
SMS076 (MG1655 (<i>crI</i> ⁺), $\Delta proQ::kan hfq-FLAG$)	this study	GSO969
PA105 (MG1655 (<i>crI</i> ⁺), $\Delta rybB::kan$)	this study	GSO970
SMS105 (MG1655 (<i>crI</i> ⁺), <i>rybB-M1::kan</i>)	this study	GSO961
SMS106 (MG1655 (<i>crI</i> ⁺), <i>rybB-M2::kan</i>)	this study	GSO962
AZ674 (MG1655 (<i>crI</i> ⁺), $\Delta rbsZ::kan$)	this study	GSO965
AZ675 (MG1655 (<i>crI</i> ⁺), $\Delta rbsZ-S::kan$)	this study	GSO966
SMS133 (MG1655 (<i>crI</i> ⁺), $\Delta rmc::cat$)	this study	GSO971
SMS136 (MG1655 (<i>crI</i> ⁺) <i>rne-3071 zce-726::Tn102</i>)	this study	GSO972
PA163 (MG1655 (<i>crI</i> ⁺), $\Delta mr::kan$)	this study	GSO973
SMP268 (NEB5 α + pSUB11)	Uzzau et al., 2001	N/A
SMP269 (NEB5 α + pKD4)	Datsenko and Wanner, 2000	N/A
SMP046 (TOP10 + pCP20)	Cherepanov and Wackernagel, 1995	N/A
SMP252 (NEB5 α + pBAD33)	Guzman et al., 1995	N/A
AZ321 (JM109 + pBRplac)	Guillier and Gottesman, 2006	N/A
AZ324 (JM109 + pBRplac-RybB)	Coornaert et al., 2010	N/A

(Continued on next page)

Continued

REAGENT or RESOURCE	SOURCE	IDENTIFIER
SMP276 (XL10-Gold + pBRplac-RybB-M2)	this study	GSO979
PA131 (NEB5 α + pBRplac-RbsZ)	this study	GSO974
PA132 (NEB5 α + pBRplac-RbsZ-S)	this study	GSO975
PA133 (NEB5 α + pBRplac-RbsZ-M1)	this study	GSO976
PA139 (NEB5 α + pBRplac-RbsZ-M2)	this study	GSO977
SMP253 (NEB5 α + pBAD33-proQ)	this study	GSO978
SMP274 (NEB5 α + pXG10-SF-rbsB)	this study	GSO980
SMP281 (NEB5 α + pXG10-SF-rbsB-M2)	this study	GSO981
Chemicals, Peptides, and Recombinant Proteins		
TRIZol Reagent	Thermo Fisher Scientific	Cat#15596018
RIL-seq reagents	Melamed et al., 2018	N/A
212-300 μ m Glass Beads	Sigma-Aldrich	Cat#G1277
Protein A-Sepharose CL-4B	GE Healthcare	Cat#17-0780-01
RNase A and RNase T1	Thermo Fisher Scientific	Cat#EN0551
Pierce Protein A/G Magnetic Beads	Thermo Fisher Scientific	Cat#88803
Ureagel-8	National Diagnostics	Cat#EC-838
Ureagel Complete	National Diagnostics	Cat#EC-841
NuSieve 3:1 Agarose	Lonza	Cat#50090
37% Formaldehyde	Fisher Scientific	Cat#BP531-500
RiboRuler High Range RNA Ladder	Thermo Fisher Scientific	Cat#SM1821
RiboRuler Low Range RNA Ladder	Thermo Fisher Scientific	Cat#SM1831
Zeta-Probe Blotting Membrane	Bio-Rad	Cat#1620159
ULTRAhyb-Oligo Hybridization Buffer	New England Biolabs	Cat#AM8663
γ - ³² P ATP	PerkinElmer	Cat#NEG035C010MC
T4 Polynucleotide Kinase	New England Biolabs	Cat#M0201L
Illustra MicroSpin G-50 Columns	GE Healthcare	Cat#27533001
Mini-PROTEAN TGX Gels	Bio-Rad	Cat#456-1086
Nitrocellulose Membrane	Thermo Fisher Scientific	Cat# LC2000
Alkaline Phosphatase, Calf Intestinal (CIP)	New England Biolabs	Cat#M0290S
RNase III	Thermo Fisher Scientific	Cat#AM2290
GlycoBlue Coprecipitant	Thermo Fisher Scientific	Cat#AM9515
Critical Commercial Assays		
QuikChange Lightning Site-Directed Mutagenesis Kit	Agilent	Cat#210519
Amersham ECL Western Blotting Detection Kit	GE Healthcare	Cat#RPN2108
MEGAscript T7 High Yield Transcription Kit	Thermo Fisher Scientific	Cat#AM1354
Ambion RNase T1 Kit	Thermo Fisher Scientific	Cat#AM2283
Deposited Data		
Sequencing data	this study	GEO: GSE131520
Oligonucleotides		
RNA-seq oligos	Table S9	N/A
Overexpression constructs oligos	Table S9	N/A
Chromosomal variants oligos	Table S9	N/A
Structural probing sequences	Table S9	N/A
Northern Probes	Table S9	N/A
Recombinant DNA		
pSUB11	Uzzau et al., 2001	N/A
pKD4	Datsenko and Wanner, 2000	N/A

(Continued on next page)

Continued

REAGENT or RESOURCE	SOURCE	IDENTIFIER
pCP20	Cherepanov and Wackernagel, 1995	N/A
pBAD33	Guzman et al., 1995	N/A
pXG10-SF	Corcoran et al., 2012	N/A
pBRplac	Guillier and Gottesman, 2006	N/A
pBRplac-RybB	Coornaert et al., 2010	N/A
pBRplac-RybB-M2	this study	N/A
pBRplac-RbsZ	this study	N/A
pBRplac-RbsZ-S	this study	N/A
pBRplac-RbsZ-M1	this study	N/A
pBRplac-RbsZ-M2	this study	N/A
pBAD33-proQ	this study	N/A
pXG10-SF-rbsB	this study	N/A
pXG10-SF-rbsB-M2	this study	N/A
Software and Algorithms		
Python RILSeq package (versions 0.47 and 0.60)	Melamed et al., 2018	https://github.com/asafpr/RILseq
EcoCyc version 19.0	Keseler et al., 2013	http://ecocyc.org
Biopython (v1.67)	Biopython	http://biopython.org/
ImageJ software	ImageJ	http://rsb.info.nih.gov/ij
R VennDiagram package	Chen and Boutros., 2011	https://cloud.r-project.org/web/packages/VennDiagram/index.html
R RCircos Package	Zhang et al., 2013	https://cloud.r-project.org/web/packages/RCircos/index.html
Kutools	ExtendOffice	https://www.extendoffice.com/product/kutools-for-excel.html
Deposited data		
Unprocessed and uncompressed imaging data	Mendeley Data	https://data.mendeley.com/datasets/srfczk4whb/1

LEAD CONTACT AND MATERIALS AVAILABILITY

Further information and requests for resources and reagents should be directed to and will be fulfilled by the Lead Contact, Gisela Storz (storzg@mail.nih.gov).

All unique/stable reagents generated in this study are available from the Lead Contact with a completed Materials Transfer Agreement.

EXPERIMENTAL MODEL AND SUBJECT DETAILS**Bacteria**

Descriptions of all *Escherichia coli* strains used in this study are in the Key Resources Table. Unless indicated otherwise, bacterial strains were grown with shaking at 250 rpm at 37°C in either LB rich or M63 minimal medium. Ampicillin (100 µg/mL), chloramphenicol (25 µg/mL) and kanamycin (30 µg/mL) were added where appropriate. IPTG was added at a final concentration of 1 mM. For M63 medium, carbon sources were added at a final concentration of 0.2%, with the exception of glycerol, which was present at 0.4%. Unless indicated otherwise, overnight cultures were diluted to an OD₆₀₀ of 0.05 and grown to indicated time points.

The *E. coli* strain expressing Hfq-FLAG was kindly provided by H. Margalit ([Melamed et al., 2016](#)). The *E. coli* strain expressing ProQ-3XFLAG was constructed by amplifying the 3XFLAG and *kan^R* sequence from plasmid pSUB11 ([Uzzau et al., 2001](#)) using primers AZ1403 and AZ1404. The PCR product was recombined into the chromosome of NM400 (kind gift of Nadim Majdalani) at the end of *proQ* coding sequence and transferred to MG1655 (GSO983) by P1 transduction. Recombination was verified by PCR using primers AZ1405 and SM039. The $\Delta proQ::kan$, $\Delta rbsZ::kan$ and $\Delta rbsZ-S::kan$, *rybB-M1::kan* and *rybB-M2::kan* strains were constructed by amplifying the *kan^R* sequence in pKD4 ([Datsenko and Wanner, 2000](#)) using the oligonucleotides listed in Table S9 and recombining the product into the chromosome of strain NM400 by recombineering ([Datsenko and Wanner, 2000](#)). All of the mutations were confirmed by sequencing and subsequently transferred to new backgrounds by P1 transduction. The $\Delta hfq \Delta proQ$ strain was

generated by P1 transducing $\Delta hfq::cat$ into a $\Delta proQ$ strain cured of kan^R using plasmid pCP20 (Cherepanov and Wackernagel, 1995). Mutant alleles in *E. coli* strains obtained from other groups (Baba et al., 2006; Hobbs et al., 2010; Massé et al., 2003; Yu et al., 2000), as referenced in the Key Resources Table, were also transduced into MG1655 (GSO982) by P1 transduction.

METHOD DETAILS

Plasmid construction

Descriptions of plasmids used in this study are in the Key Resources Table. All sRNAs assayed were overexpressed from pBRplac (Guillier and Gottesman, 2006). sRNA sequences were PCR amplified using the appropriate primers as listed in Table S9, digested with AatII and HindIII and cloned into pBRplac digested with the same restriction enzymes. The pBR-RbsZ mutant derivatives were obtained by cloning gBlocks (IDT) with the desired sequences into pBRplac or by site direct mutagenesis using QuikChange Lightning Site-Directed Mutagenesis Kit (Agilent). ProQ was overexpressed from pBAD33 (Guzman et al., 1995), a plasmid compatible to pBRplac. The *proQ* sequence was PCR amplified using primers SM405 and SM406, digested with KpnI and HindIII and cloned into pBAD33 digested with the same restriction enzymes. The sequences of inserts were verified. Construction of *rbsB-gfp*-fusion plasmids were carried out essentially as described in (Urban and Vogel, 2009), using the pXG10-SF (Corcoran et al., 2012) as the backbone. Briefly, the *rbsB* 5' region was PCR amplified using primers SM480 and SM481, digested with Mph1103I and NheI and cloned upstream of *gfp* in pXG10-SF digested with the same enzymes. The pXG10-SF-*rbsB* mutant derivative was generated by site-direct mutagenesis using QuikChange Lightning Site-Directed Mutagenesis Kit (Agilent).

RNA isolation

Cells corresponding to the equivalent of 10 OD₆₀₀ were collected by centrifugation, washed once with 1X PBS, and snap frozen in liquid nitrogen. RNA was extracted according to the standard TRIzol (Thermo Fisher Scientific) protocol. Briefly, 1 mL of room temperature TRIzol was added to cell pellets, resuspended thoroughly to homogenization, and incubated for 5 min at room temperature. After the addition of 200 μ l of chloroform and thorough mixing by inversion, samples were incubated for 10 min at room temperature. After samples were centrifuged for 10 min at 4°C on maximal speed, the upper phase (~0.6 ml) was transferred into a new tube and 500 μ l of isopropanol was added. Samples were mixed thoroughly by inversion, incubated for 10 min at room temperature and centrifuged at maximal speed for 15 min at 4°C. RNA pellets were washed twice with 75% ethanol. After the second wash, the ethanol was aspirated, and the RNA pellet was left to dry at room temperature. RNA was resuspended in 20-50 μ l of DEPC water and quantified using a NanoDrop (Thermo Fisher Scientific).

RIL-seq

RIL-seq was carried out essentially as previously described (Melamed et al., 2018; Melamed et al., 2016) using WT (GSO983), *hfq-FLAG* (HM34) and *proQ-3XFLAG* (GSO953) for RIL-seq experiment 1 and WT (GSO983), *hfq-FLAG* (HM34), *proQ-3XFLAG* (GSO953), $\Delta proQ$ *hfq-FLAG* (GSO969) and Δhfq *proQ-3XFLAG* (GSO960) for RIL-seq experiment 2. The libraries were sequenced by paired-end sequencing using the HiSeq 2500 system (Illumina). The computational analysis for the RIL-seq experiment 1 was done using the RIL-seq software (version 0.47). The computational analysis for the RIL-seq experiment 2 was done using the RIL-seq software (version 0.60). When the RIL-seq experiment 1 was re-analyzed with RIL-seq software (version 0.60), no significant differences were observed. Fragments were mapped to the genome of *E. coli* K12 MG1655 (RefSeq accession number NC_000913.3). Table S1 provides the statistics regarding the number of sequenced fragments for both RIL-seq experiments.

Genome annotation was based on EcoCyc version 19.0 (Keseler et al., 2013). Coding regions were termed CDS. Annotation of 5'UTRs and 3'UTRs (termed 5UTR and 3UTR in figures and tables) was based on annotation in EcoCyc. In cases where the transcription start or termination sites of a gene were unknown (termed EST3UTR/EST5UTR for estimated UTRs), the UTRs were considered as the regions 100 nt upstream the ATG and downstream the stop codon (or shorter if these regions spanned another transcript or were more likely to be a UTR of the neighboring transcript). Intergenic regions were termed IGR if their boundary genes were not in the same transcript or IGT if the two boundary genes were part of the same transcript. Ribosomal RNA and transfer RNA were denoted rRNA and tRNA, respectively. Small RNAs that exert their regulation via base-pairing with trans-encoded targets or that are candidate regulatory RNAs as denoted by EcoCyc were grouped as sRNAs. The 4.5S RNA, RNase P RNA and tmRNA encoded by *ffs*, *mpB* and *ssrA* were also included in this category. Transcripts antisense to genes or to IGT were termed AS and AS_IGT respectively. The same annotation was maintained in all tables and figures unless noted otherwise. However since the annotation is done automatically and uses rigid rules to assign each RNA a single annotation, there are inevitably some mis-annotations.

RNA-seq

Total RNA was extracted as indicated earlier. Library construction was carried out based on the RNAtag-Seq methodology (Shishkin et al., 2015), which was adapted to capture bacterial sRNAs (Melamed et al., 2018). The libraries were sequenced by paired-end sequencing using the HiSeq 2500 system (Illumina). RNA-seq data processing follows the same procedures as RIL-seq data analysis for QC analysis, adaptor removal, and alignment with the Python RILSeq package. All fragment files were generated in parallel with the RIL-seq files. Table S1 provides the statistics regarding the number of sequenced fragments for all RNA-seq libraries.

RNA coimmunoprecipitation (Co-IP) assay

Polyclonal antibodies to Hfq were generated previously by immunizing rabbits with purified *E. coli* Hfq protein (Zhang et al., 2002). Polyclonal antibodies to ProQ were generated by immunizing rabbits with purified His-tagged *E. coli* ProQ protein (Biosynthesis). RNAs that co-IP with Hfq or ProQ were isolated as described previously (Zhang et al., 2002) with the following modifications. MG1655 (GSO982), $\Delta hfq::cat-sacB$ (GSO954), or $\Delta proQ::kan$ (GSO956) cells were grown to $OD_{600} \sim 10$ in LB medium. Cells corresponding to the the equivalent of 20 OD_{600} were collected, and cell lysates were prepared by vortexing with 212–300 μm glass beads (Sigma-Aldrich) in a final volume of 1 mL lysis buffer (20 mM Tris-HCl/pH 8.0, 150 mM KCl, 1 mM MgCl_2 , 1 mM DTT). Co-IPs were carried out using either 100 μL of α -Hfq or 10 μL of α -ProQ antibody, 120 mg of protein A-Sepharose beads (GE Healthcare), and 950 μL of cell lysate. Co-IP RNA was isolated from protein A-Sepharose beads by extraction with phenol:chloroform:isoamyl alcohol (25:24:1), followed by ethanol precipitation. Total RNA was isolated from 50 μL of cell lysate by TRIzol (Thermo Fisher Scientific) extraction followed by chloroform extraction and isopropanol precipitation. Total and co-IP RNA samples were resuspended in 15 μL of DEPC H_2O and 1 μL of each were subjected to Northern analysis as described below.

Protein coimmunoprecipitation (Co-IP) assay

Co-IP of Hfq and ProQ proteins was performed using the initial steps of the RIL-seq protocol (Melamed et al., 2018) without UV-cross-linking. Cells corresponding to the the equivalent of 40 OD_{600} were collected in duplicate. Following lysis, one set of samples was incubated with 2 μg RNase A and 5 U RNase T1 (Thermo Fisher Scientific) for 15 min at 22° C. Co-IPs were carried out for both samples using 3 μg monoclonal anti-FLAG M2 antibody (Sigma-Aldrich) and 20 μL of Pierce protein A/G magnetic beads (Thermo Fisher Scientific). Aliquots of total lysate, IP lysate, and IP lysate treated with RNases were mixed with equal volume 2X Laemmli sample buffer (Bio-Rad) and subjected to immunoblot analysis as described below.

Northern blot analysis

For shorter RNAs, equal amounts (5–10 μg) of total RNA were fractionated on 8% polyacrylamide urea gels containing 6 M urea (1:4 mix of Ureagel Complete to Ureagel-8 (National Diagnostics) with 0.08% ammonium persulfate) in 1X TBE buffer at 300V for 90 min. The RNA was transferred to a Zeta-Probe GT membrane (Bio-Rad) at 20 V for 16 h in 0.5X TBE. For longer RNAs, the indicated amounts of total RNA were fractionated on formaldehyde-MOPS agarose gels as previously described (Adams et al., 2017). Briefly, RNA was denatured in 3.7% formaldehyde (Fisher), 1X MOPS (20 mM MOPS, 5 mM NaOAc, 1 mM EDTA, pH 7.0) and 1X RNA loading dye (Thermo Fisher Scientific) for 10 min at 70°C and incubated on ice. The RNA was loaded onto a 2% NuSieve 3:1 agarose (Lonza), 1X MOPS, 2% formaldehyde gel and separated at 125–150V at 4°C for 1–2 h and then transferred to a Zeta-Probe GT membrane (Bio-Rad) via capillary action overnight (Streit et al., 2009).

For both types of blots, the RNA was crosslinked to the membranes by UV irradiation. RiboRuler High Range and Low Range RNA ladders (Thermo Fisher Scientific) were marked by UV-shadowing. The membranes were then blocked in ULTRAhyb-Oligo Hybridization Buffer (Ambion) for 2 h at 45° C. Oligonucleotide probes (listed in Table S9), were 5' ^{32}P -end labeled with 0.3 mCi of γ - ^{32}P ATP (Perkin Elmer) by incubating with 10 U of T4 polynucleotide kinase (New England Biolabs) at 37° C for 1 h. Subsequently, labeled probes were purified using Illustra MicroSpin G-50 columns (GE Healthcare) and 40 pmol of these probes was added to the blocked membranes. After an overnight incubation, the membranes were rinsed twice with 2X SSC/0.1% SDS at room temperature, once with 0.2X SSC/0.1% SDS at room temperature, washed for 25 min with 0.2 \times SSC/0.1% SDS at 45° C, followed by a final rinse with 0.2X SSC/0.1% SDS at room temperature prior to exposure. Blots were stripped by three, 7 min incubations in boiling 0.2% SDS followed by three, 7 min incubations in boiling water.

Immunoblot analysis

Immunoblot analysis was performed as described previously with minor changes (Zhang et al., 2002). Samples were separated on a Mini-PROTEAN TGX 5%–20% Tris-Glycine gel (Bio-Rad) and transferred to a nitrocellulose membrane (Thermo Fisher Scientific). Membranes were blocked in 1X PBST containing 3% milk, probed with a 1:5,000 dilution of α -Hfq or a 1:10,000–1:20,000 dilution of α -ProQ antibody, followed by incubation with a 1:20,000 dilution of peroxidase labeled anti-rabbit antibody and detection with a Amersham ECL Western Blotting Detection Kit (GE Healthcare).

RNA structure probing

gBlock fragments carrying the RybB, RybB M1, RbsZ-S and RbsZ-S M1 sequences (listed in Table S9) were synthesized (IDT) and 2 pmol of each were used as DNA templates for *in vitro* transcription with MEGAscript T7 High Yield Transcription Kit (Thermo Fisher Scientific). Reactions were purified using Illustra MicroSpin G-50 columns (GE Healthcare) and 50 pmol of each transcript were dephosphorylated with 10 U CIP (New England Biolabs) and radioactively labeled at 5' end with 0.17 mCi of γ - ^{32}P ATP (Perkin Elmer) and 10 U T4 kinase (New England Biolabs). Labeled RNAs were purified using Illustra MicroSpin G-50 columns (GE Healthcare) and separated on a 8% polyacrylamide/6M urea gel. Full length transcripts were excised and eluted in 750 μL RNA elution buffer (20 mM Tris-HCl/pH 7.5, 0.5 M NaOAc, 10 mM EDTA, 1% SDS) at 4° C overnight, followed by ethanol precipitation. The RNA concentration was determined using an Agilent 4200 TapeStation System. For all structural probing assays, 0.2 pmol of the labeled transcript, 2 pmol of unlabeled transcript and 1 μg of yeast RNA were mixed in 10 μL of 1X Structural Buffer using the Ambion RNase T1 Kit (Thermo Fisher Scientific). The reactions were incubated at 37° C for 1 h, followed by treatment at 37° C with 1.3 U RNase III (Thermo

Fisher Scientific) for 3 min, 10 min or 20 min, whereupon 20 μ l Inactivation Buffer and 15 μ g Glycoblue (Thermo Fisher Scientific) were added. The RNAs were precipitated and resuspended in 7 μ l Gel Loading Buffer II and analyzed on an 8% polyacrylamide/6 M urea gel run in 1X TBE. RNase T1 and alkali digestion of the end-labeled transcripts were used as molecular size markers.

GFP reporter assay

The GFP reporter assay was principally done as described previously (Corcoran et al., 2012; Urban and Vogel, 2009). MG1655 (GSO982) cells were transformed with a *rbsB-gfp* reporter plasmid and with RybB overexpressing plasmid or pBRplac as a control. Single colonies were grown overnight at 37°C in LB supplemented with ampicillin and chloramphenicol. The cultures were diluted to OD₆₀₀ = 0.05 in fresh medium supplied with 1 mM IPTG and grown at 37°C for 3 h in a 96 deep-well plate. An aliquot (1 ml) of each culture was centrifuged and the pellet was resuspended in 220 μ l of 1X PBS. Fluorescence was measured using the CytoFLEX Flow Cytometer (Beckman Coulter). Three biological repeats were analyzed for every sample.

QUANTIFICATION AND STATISTICAL ANALYSIS

Spearman correlation between libraries

The reproducibility of the results within same-condition libraries was evaluated for all S-chimeras and for all single and chimeric fragments. Briefly, for each library, the sequenced fragments were mapped to 100 nt-long windows along the genome, as described previously (Melamed et al., 2016), and the Spearman correlation coefficient in number of mapped fragments in corresponding genomic windows between each pair of libraries was calculated.

RNA enrichment in RIL-seq libraries

RIL-seq library reads and total RNA library reads were normalized by the total number of reads in the library (RPM). One read was added to each RNA in order to reduce the background noise. IP enrichment for each RNA was calculated by dividing its normalized number of reads in RIL-seq libraries with the normalized number of reads in the corresponding total RNA library. The average IP enrichment value of two biological repeats for each condition tested was then calculated.

Cutoffs for chimeras in RIL-seq libraries

Statistically significant chimeras (S-chimeras) were determined as previously described (Melamed et al., 2018). We applied the following additional threshold for the S-chimeras in RIL-seq experiment 1. We sorted Table S5 according to the number of chimeric fragments and eliminated those S-chimeras which had less than 39 chimeric fragments for Hfq-FLAG and ProQ-3XFLAG cells grown in LB and less than 60 chimeric fragments or more for cells grown in M63. These cutoffs eliminate 90% of the S-chimeras in the control libraries (*E. coli* with untagged Hfq and ProQ). For example, there were 52 different S-chimeras for the LB WT control. When these are ranked by the number of chimeric fragments, 90% had fewer than 39 fragments. There was only one S-chimera in the control libraries for the RIL-seq experiment 2. Therefore, we did not apply another threshold for the S-chimeras in the ProQ-3XFLAG or Hfq-FLAG libraries, and all S-chimeras with 5 or more fragments were analyzed.

Venn diagrams

Venn diagrams of S-chimeras between two different groups are generated with R VennDiagram package (Chen and Boutros, 2011).

Circos plots

Circos plots follow the procedures of RCircos Package (Zhang et al., 2013). Link lines are used to label the S-chimeras and total of 5 transparent levels (0.4, 0.55, 0.7, 0.85, and 1) of line colors are used to represent the log₁₀ values of total interactions supporting the S-chimera (the more of total interactions, the higher of the color density).

Browser images

Data from RIL-seq experiment 2 extracted for unified S-chimeras files for RybB were mapped based on the first nt of each read in the chimera. BED files are generated with Python RILSeq package (Melamed et al., 2018). For RNA already annotated in GTF file, BED files are directly generated with command of generate_BED_file_of_endpoints.py and EcoCyc ID. For newly annotated genes, significant chimeras which involve the relevant gene are first extracted from significant interaction file, then chimeric reads involving the S-chimeras are extracted from chimeric read file. To be a qualified chimeric read, RNA1 start position of the read must overlap with the genomic range of RNA1 in S-chimera and RNA2 start position of the read must overlap with the genomic range of RNA2 in S-chimera. Finally, the read list for newly annotated gene are supplied to generate_BED_file_of_endpoints.py command to generate BED file.

Free energy of hybridization calculations

RNAup tools in ViennaRNA package (Lorenz et al., 2011) were used to calculate hybridization energy for each RNA pair in chimeric fragments. For each RNA, target sequences were extracted based on the genome coordinates of the RNA in the chimeric fragment

with an additional 20 nt upstream of the first read and downstream of the last read. Probability of unpaired regions in both RNAs was used for calculation. The default was used for all other parameters.

Recognition of sequence motifs

Common binding motifs of same experiment condition were searched with MEME software (Bailey et al., 2009). For each chimeric fragment, genomic sequences of RNA1 and RNA2 were extracted using the coordinates for the start of the first read and start of the last read of each RNA, respectively, with 50 nt added to both sides of the sequence. Overlapping sequences were merged as one and all "T" bases were replaced by "U." The motif search was applied for RNA1 and RNA2 separately for each experimental condition. For outputs, motif length was restricted to 15 and number of motifs was limited to 10.

Functional annotation analysis

Functional annotation analysis was carried out using the Database for Annotation, Visualization and Integrated Discovery (DAVID) (Huang da et al., 2009). Gene names and 5'UTRs served as the input list in each case. The following datasets from the 1st RIL-seq experiment were analyzed: Overlapping RNA pairs in LB, Hfq-LB dataset, Hfq-LB unique RNA pairs, ProQ-LB and ProQ-LB unique RNA pairs.

DATA AND CODE AVAILABILITY

The sequencing data reported in this paper have been deposited in GEO under accession number GSE131520.

The RIL-seq data generated in this study is available online via UCSC genome browser at the following links:

RIL-seq experiment 1:

https://genome.ucsc.edu/cgi-bin/hgTracks?hubUrl=https://hpc.nih.gov/~NICHD-core0/storz/trackhubs/ecoli_rilseq/hub.txt&hgS_loadUrlName=https://hpc.nih.gov/~NICHD-core0/storz/trackhubs/ecoli_rilseq/session.txt&hgS_doLoadUrl=submit

RIL-seq experiment 2:

https://genome.ucsc.edu/cgi-bin/hgTracks?hubUrl=https://hpc.nih.gov/~NICHD-core0/storz/trackhubs/ecoli_rilseq2/hub.txt&hgS_loadUrlName=https://hpc.nih.gov/~NICHD-core0/storz/trackhubs/ecoli_rilseq2/session.txt&hgS_doLoadUrl=submit

The different tracks are displayed simultaneously using UCSC's Track Hub functionality. Python trackhub library was used for creating, organizing, and uploading tracks into UCSC hubs.

Chimeras

Output from RIL-seq pipeline as BED files. Colors used are those from the original RIL-seq files where red is 5' and blue is 3'. RIL-seq reports the read names as feature IDs, which are retained here for consistency.

Coverage

BigWig versions of the chimera tracks described above. These better show high signal and/or wide dynamic range at large genomic intervals. The colors match the chimera tracks above.

IP and total

Output from RIL-seq pipeline as stranded WIG files, which were converted to bigWig for incorporation into the track hub. The y axis units depend on the RIL-seq pipeline. Plus-strand signal is shown as positive values, and minus-strand signal is shown as negative values. The tracks are auto-scaled by default. Multiple replicates are shown as transparent overlays of the same color. IP tracks are in purple and total tracks are shown in black. Not all IPs are shown by default, and not all totals are shown by default.

Annotations

Genes from EcoCyc, converted to bigBed and indexed so that the genes can be searched for through the browser.

Pairs

From Excel file output from RIL-seq pipeline, extracted each side of the detected pair, and named features according to their gene pair. The gene in which the fragments is located is listed first, and the paired gene is listed after the "/." The resulting bigBed files are indexed to enable searching for either side of a chimera. Used total RNA reads as score; log-transformed, divided by max, and then multiplied by 1000 to conform to UCSC score range requirements of 0-1000.

Mendeley Data

Unprocessed and uncompressed imaging data have been deposited to Mendeley Data and are available at: <https://data.mendeley.com/datasets/srfczk4whb/1>.

Molecular Cell, Volume 77

Supplemental Information

**RNA-RNA Interactomes of ProQ and Hfq
Reveal Overlapping and Competing Roles**

Sahar Melamed, Philip P. Adams, Aixia Zhang, Hongen Zhang, and Gisela Storz

Supplemental Information

Table of Contents

Supp. Figure S1. Evaluation of conditions for RIL-seq and correlation between RIL-seq libraries (for Figure 1)

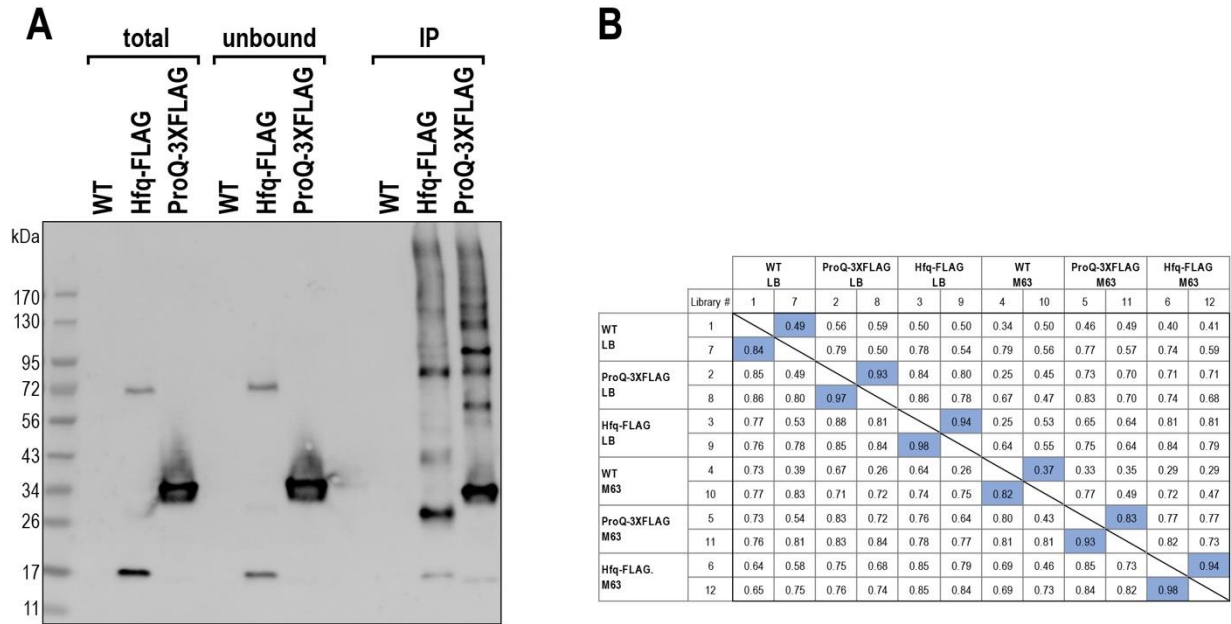
Supp. Figure S2. Growth of Δhfq , $\Delta proQ$ and $\Delta hfq \Delta proQ$ mutants and effects of $\Delta proQ$ on RNA expression (for Figure 2)

Supp. Figure S3. Impact of 90% threshold on RIL-seq chimera data and results for cells grown in M63 (for Figure 3)

Supp. Figure S4. Hfq and ProQ do not interact directly (for Figure 4)

Supp. Figure S5. Elevated RbsZ-S in ribose and effects of RbsZ-S and $\Delta rbsZ$ (for Figures 5, 6 and 7)

SUPPLEMENTARY FIGURES



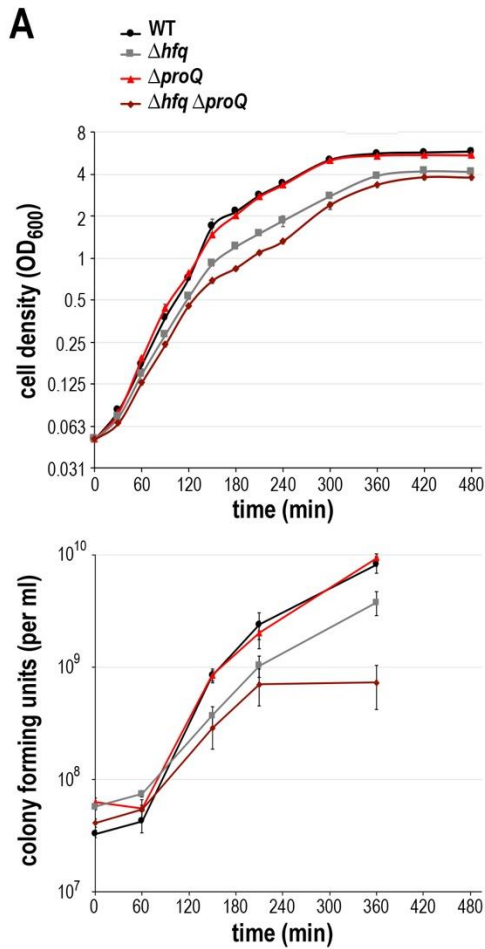
Supp. Figure S1. Evaluation of conditions for RIL-seq and correlation between RIL-seq libraries

(related to Figure 1)

(A) Immunoblot assay of Hfq-FLAG and ProQ-3XFLAG immunoprecipitated after cross-linking. Strains expressing Hfq-FLAG (HM34) and ProQ-3XFLAG (GSO953) as well as a WT control strain (GSO983) were grown to $OD_{600} \sim 1.0$, the cells were exposed to $80,000 \mu\text{J}/\text{cm}^2$ UV irradiation to generate protein-RNA crosslinks, and cell lysates were prepared. The lysates were subjected to IP assay using magnetic beads carrying M2 anti-FLAG monoclonal antibody. The lysates, unbound fraction, and bound fraction (IP) were examined by immunoblot analysis using anti-FLAG antibody.

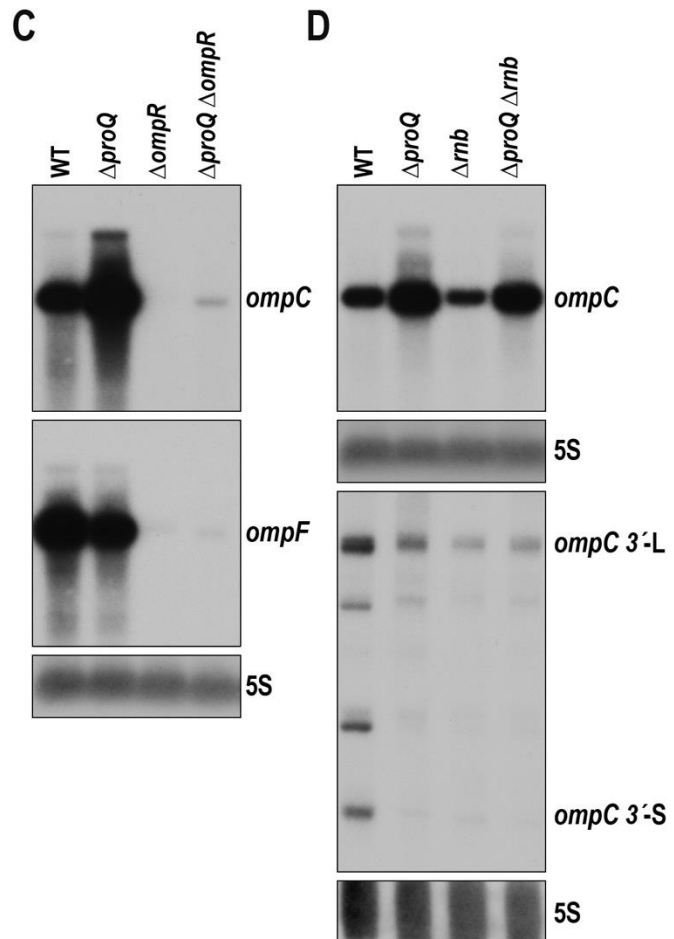
(B) Correlation in number of mapped sequenced fragments in corresponding genomic windows between same-condition libraries (blue shading). The reproducibility of the results within same-condition libraries was evaluated for all statistically significant chimeric fragments (S-chimeras)

(cells above the diagonal) and for all single and chimeric fragments (cells below the diagonal). The numbers of fragments mapped to a 100 nt long region of the genome in two libraries were analyzed. The Spearman correlation coefficients are reported for each cell. The libraries correspond to those listed in Table S1.



B

		WT			$\Delta proQ$		
	Library #	1	2	3	4	5	6
WT	1						
	2	0.95					
	3	0.95	0.95				
	4	0.94	0.95	0.95			
$\Delta proQ$	5	0.94	0.94	0.95	0.96		
	6	0.94	0.94	0.95	0.96	0.96	



Supp. Figure S2. Growth of Δhfq , $\Delta proQ$ and $\Delta hfq \Delta proQ$ mutants and effects of $\Delta proQ$ on RNA expression

(related to Figure 2)

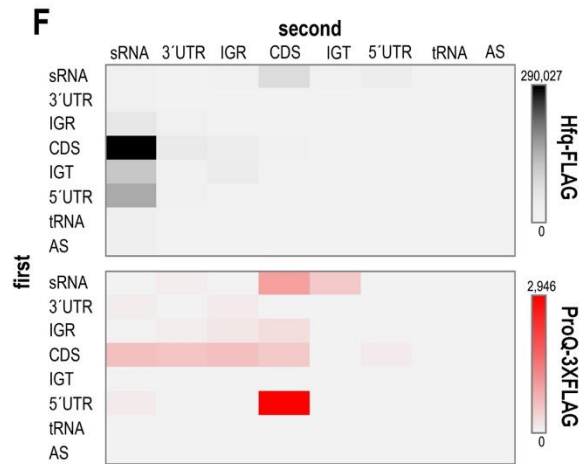
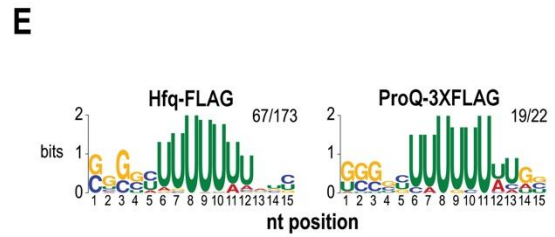
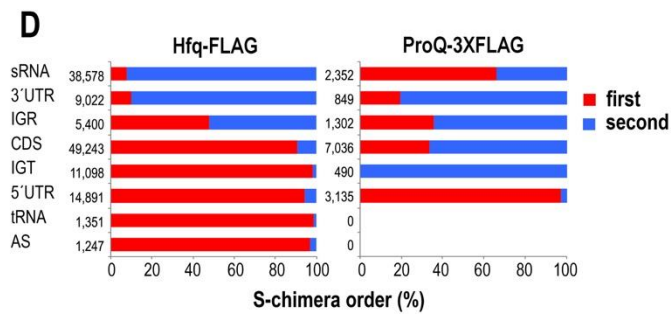
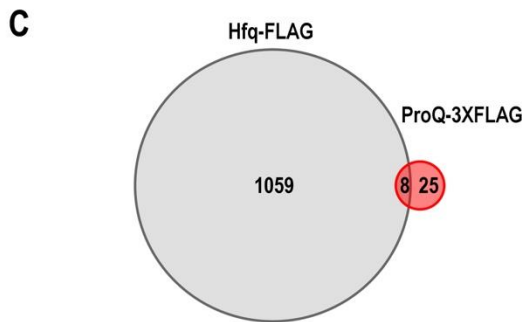
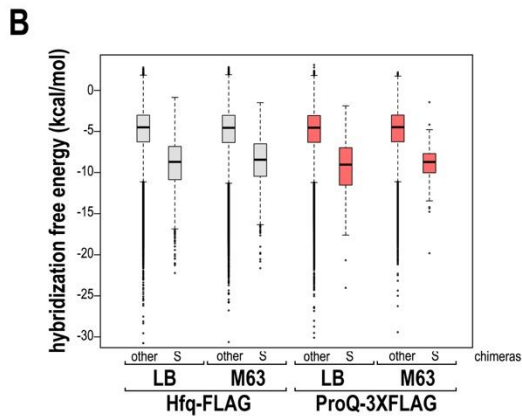
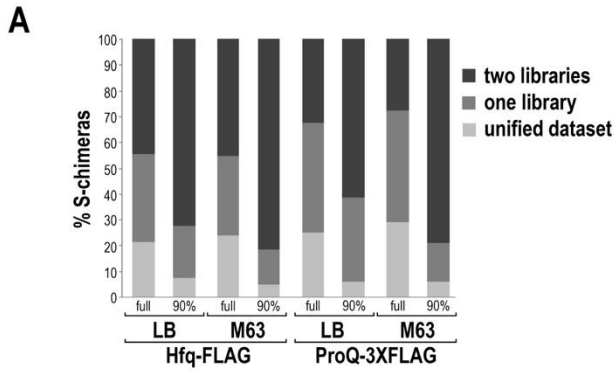
(A) Growth curves of WT (GSO982), Δhfq (GSO954), $\Delta proQ$ (GSO956) and $\Delta hfq \Delta proQ$ (GSO957) in LB medium. Overnight cultures were diluted to $OD_{600} = 0.05$ and cell growth was monitored for 480 min by OD_{600} measurements. Viable counts were determined at 0, 60, 180,

240 and 360 min. All points give the average of three biological replicates with the standard deviation.

(B) Correlation in number of mapped sequenced fragments in corresponding genomic windows between same-condition libraries (blue shading). The reproducibility of the results within same-condition libraries was evaluated at the level of mapped fragments. Comparison of the sequenced fragments between three libraries is shown. The numbers of fragments mapped to a 100 nt long region of the genome in three libraries were analyzed. The Spearman correlation coefficients are reported for each cell. The libraries correspond to those listed in Table S4.

(C) Northern analysis showing that some effects of $\Delta proQ$ on *ompC* mRNA levels were independent of OmpR. Total RNA was extracted from WT (GSO982), $\Delta proQ$ (GSO958), $\Delta ompR$ (GSO967), $\Delta proQ \Delta ompR$ (GSO963) strains after 150 min after dilution of the overnight culture, separated on an agarose gel and sequentially probed for the *ompC*, *ompF* and 5S RNAs.

(D) Control northern analysis for 5S RNA levels for the membranes probed in Figure 2E. The *ompC* and *ompC* 3' panels of Figure 2E are repeated here.



G

chimeras	Hfq-FLAG	ProQ-3XFLAG
<i>hisL.hisG.IGT / chiX</i>	38,673	-
<i>grcA / spf</i>	24,266	-
<i>nlpD / dsrA</i>	16,871	-
<i>yebO / cyaR</i>	15,909	133
<i>ompA-5' / micA</i>	13,070	-
<i>eptB-5' / mgrR</i>	12,675	-
<i>gatZ / chiX</i>	11,916	-
<i>rbsD / arcZ</i>	10,400	-
<i>ptsG / cyaR</i>	7,897	-
<i>glmS.glmU.IGT / glmZ.hemY.IGR</i>	7,518	-
<i>ypfM / arcZ</i>	6,880	-
<i>dmsA-5' / ryhB</i>	6,316	-
<i>sstT-5' / gcvB</i>	5,963	-
<i>ompT / arcZ</i>	5,608	-
<i>fliC / mgrR</i>	5,422	-
<i>cspA-5' / raiZ</i>	-	2,094
<i>lpp-5' / raiZ</i>	-	852
<i>rybB / rbsZ</i>	154	490
<i>fruA / psuK.fruA.IGR</i>	76	466
<i>grcA / mcaS</i>	-	339
<i>ryjB / fbaA</i>	-	293
<i>ryjD / raiZ</i>	-	244
<i>ptsG / cspE-3'</i>	-	232
<i>aroG / cspE</i>	65	208
<i>micA / hupB</i>	742	188
<i>grcA / cspE</i>	-	173
<i>recE.recC.IGR / grcA</i>	-	171
<i>firS / ahpF</i>	623	125
<i>rbsB / cspE-3'</i>	-	120

Supp. Figure S3. Impact of 90% threshold on RIL-seq chimera data and results for cells grown in M63

(related to Figure 3)

(A) The percentage of S-chimeras that were found in two libraries (dark gray), one library (gray), or the unified dataset (light gray) for all four samples of RIL-seq experiment 1 for the full datasets and after the application of a “90% cutoff”. The cutoff corresponds to the number of chimeras for which 90% of the S-chimeras in the control libraries (*E. coli* with untagged Hfq and ProQ) are eliminated when table is sorted according to the number of chimeric fragments. We used this threshold for further analysis of S-chimeras in the ProQ-3XFLAG or Hfq-FLAG libraries and thus only considered interactions supported by 39 chimeric fragments or more for cells grown in LB and 60 chimeric fragments or more for cells grown in M63 (see STAR methods for more details). The chart illustrates how the cutoff enriches for the chimeras found in two libraries.

(B) Summary of computed hybridization free energy (kcal/mol) using RNAup for statistically significant chimeras (≥ 39 chimeric fragments in LB dataset and ≥ 60 in M63 dataset) and other chimeras that did not pass the threshold for statistical significance.

(C) Venn diagram showing ~24% of the RNA pairs found on ProQ-3XFLAG in M63 are shared with Hfq-FLAG M63 dataset. Only chimeras with unique names were counted.

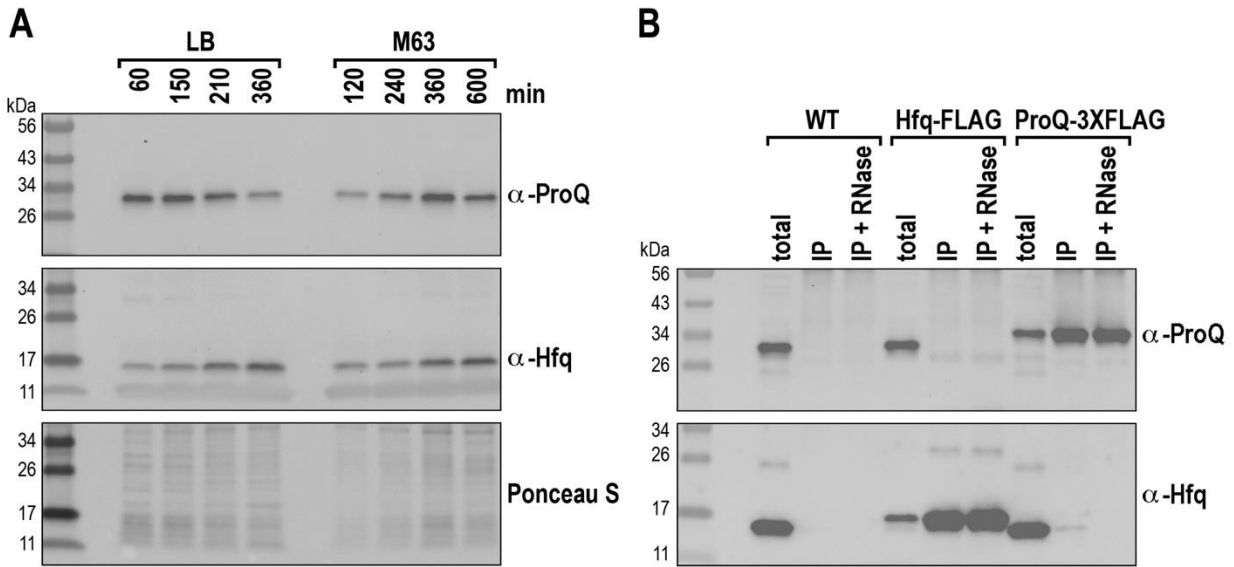
(D) Distribution of RNA locations as first (red) and second (blue) in chimeric fragments for RNAs derived from various genomic elements in Hfq M63 and ProQ M63 datasets.

(E) Motifs found for second RNA in Hfq M63 ($E = 1.7 \times 10^{-40}$) and ProQ M63 ($E = 3.5 \times 10^{-17}$) datasets. Fractions correspond to number of sequences containing motif, over the total number analyzed.

(F) Total number of chimeric fragments for each combination of genomic elements in the M63 chimera dataset of Hfq-FLAG (top) or ProQ-3XFLAG (bottom). Mapped fragments were classified as in Figure 1A. Rows represent the first RNA in the chimera and columns represent the second RNA in the chimera. In the Hfq dataset, the most prominent pairs are sRNAs with CDS or 5' UTR whereas in the ProQ dataset other combinations are also abundant.

(G) The top 15 chimeras in Hfq and ProQ M63 datasets, when table is sorted by the number of chimeras, are different. The only pair that found in both sets is *yebO-CyaR*. The enrichment value is given with the boxes for the top 15 most-enriched RNAs shaded according to the key.

For (E), (F) and (G) classifications are as in Figure 1A.



C

		WT		Hfq-FLAG		ProQ-3XFLAG		Δ proQ Hfq-FLAG		Δ hfq ProQ-3XFLAG	
	Library #	1	2	3	4	5	6	7	8	9	10
WT	1										
	2	0.79									
Hfq-FLAG	3	0.58	0.64		0.86	0.42	0.40	0.79	0.76	0.28	0.29
	4	0.60	0.66	0.96		0.41	0.40	0.82	0.79	0.27	0.29
ProQ-3XFLAG	5	0.66	0.72	0.82	0.83		0.78	0.36	0.36	0.56	0.56
	6	0.65	0.72	0.83	0.83	0.95		0.36	0.35	0.57	0.57
Δ proQ Hfq-FLAG	7	0.53	0.59	0.92	0.92	0.77	0.77		0.86	0.24	0.26
	8	0.52	0.57	0.91	0.91	0.75	0.76	0.96		0.24	0.25
Δ hfq ProQ-3XFLAG	9	0.61	0.68	0.79	0.79	0.89	0.90	0.74	0.74		0.76
	10	0.61	0.67	0.79	0.79	0.89	0.90	0.74	0.74	0.96	

Supp. Figure S4. Hfq and ProQ do not interact directly

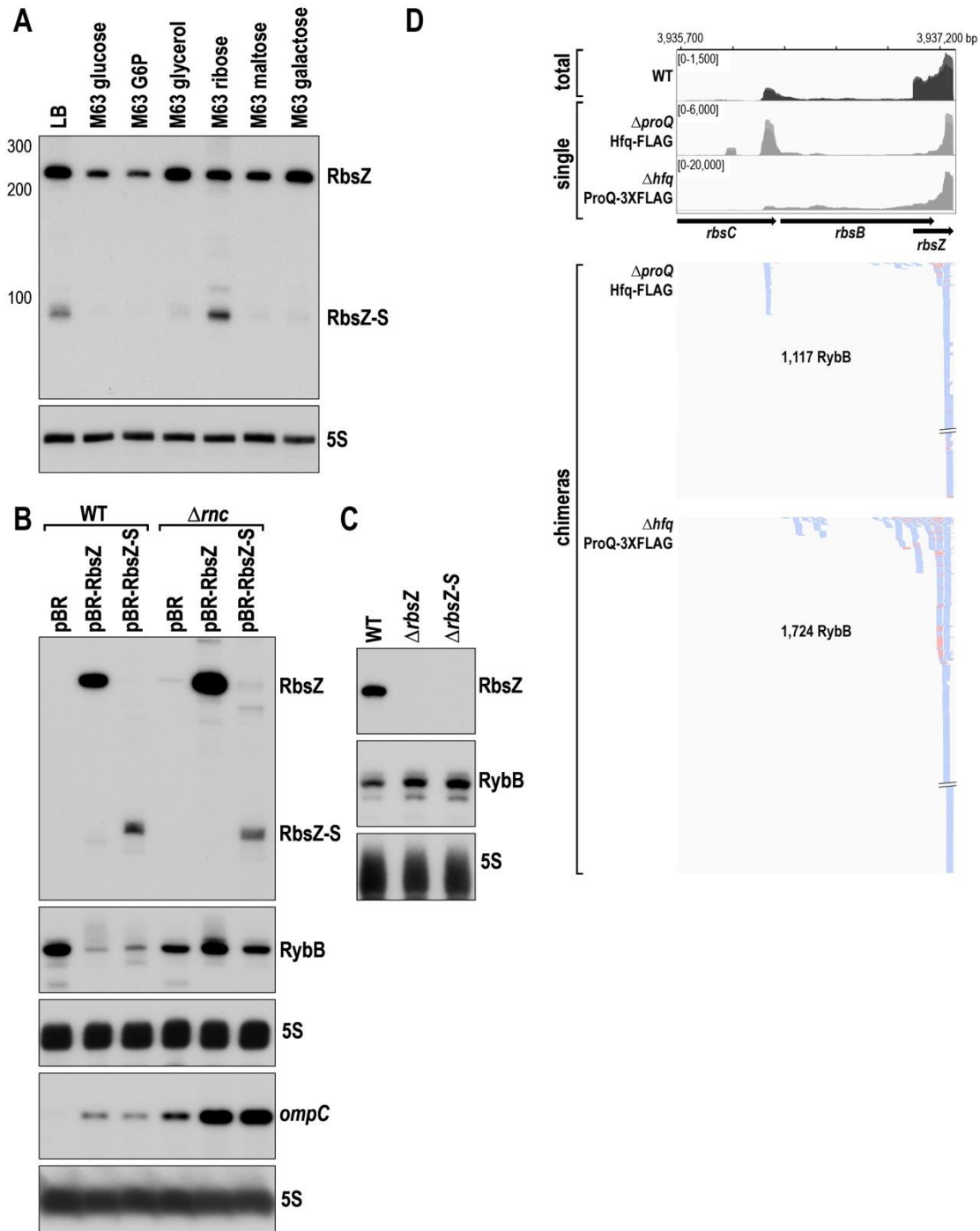
(related to Figure 4)

(A) Relative levels of ProQ and Hfq for cells grown 60, 150, 210 and 360 min after dilution in LB and for 120, 240, 360 and 600 min after dilution in M63 with 0.2% glucose were determined by immunoblot analysis using α -ProQ or α -Hfq antibodies.

(B) Immunoblot analysis using α -ProQ or α -Hfq antibodies of immunoprecipitated Hfq-FLAG (HM34) or ProQ-3XFLAG (GSO953) imply that there is no direct interaction between Hfq and

ProQ for samples taken at 360 min. Some of the IP samples were also subjected to treatment with a mix of RNase A and RNase T1.

(C) Correlation in number of mapped sequenced fragments in corresponding genomic windows between same-condition libraries (blue shading). The reproducibility of the results within same-condition libraries was evaluated as described in the legend of Figure S1B. Each cell above the diagonal shows these results for S-chimeras. The Spearman correlation coefficients are reported for each cell. The name of a library includes the condition and library number listed in Table S7.



Supp. Figure S5. Elevated RbsZ-S in ribose and effects of RbsZ-S and $\Delta rbsZ$ (for Figures 5, 6 and 7)

(A) Total RNA was extracted from WT (GSO982) grown to exponential phase ($OD_{600} \sim 0.6$) in LB medium or M63 minimal medium supplemented with 0.2% of glucose, glucose-6-phosphate

(G6P), ribose, maltose or galactose or 0.4% glycerol, separated on an acrylamide gel and sequentially probed for the RbsZ and 5S RNAs.

(B) Total RNA was extracted from WT (GSO982), Δrnc (GSO971) harboring the indicated plasmids after 360 min after dilution of the overnight culture. RNA was separated on either an acrylamide gel, transferred to a membrane, and sequentially probed for the RbsZ, RybB, and 5S RNAs or an agarose gel, transferred to a membrane, and sequentially probed for the *ompC* and 5S RNAs.

(C) Total RNA was extracted from WT (GSO982), $\Delta rbsZ$ (GSO965) and $\Delta rbsZ-S$ (GSO966) strains 360 min after dilution of the overnight culture, separated on an acrylamide gel and sequentially probed for the RbsZ, RybB and 5S RNAs.

(D) Browser image for Hfq-FLAG data in $\Delta proQ$ mutant strain and ProQ-3XFLAG data in Δhfq mutant strain from RIL-seq experiment 2 for 3,935,700-3,937,200 region of the *E. coli* chromosome. Top: Signal for WT total RNA (dark gray) and Hfq/ProQ RIL-seq enriched fragments in two biological repeats are overlaid (light gray). Read count ranges are shown in the upper left of each frame. Bottom: chimeras with RybB in unified datasets. Red and blue lines indicate RbsZ is first or second RNA in the chimera, respectively.